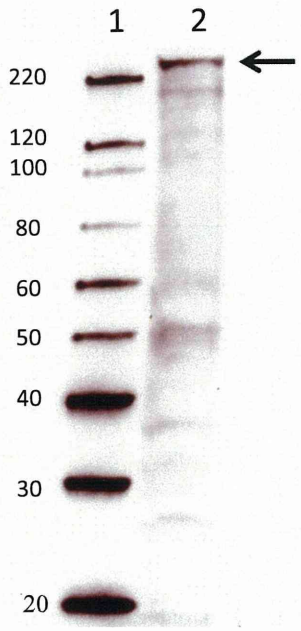

Fig. 4 Western blotting for fatty acid synthase (FASN) in U373MG cells. Lane 1: MagicMark™ XP Western Protein Standard (Life Technologies, Waltham, MA, USA). Lane 2: The arrow indicates the band for FASN.

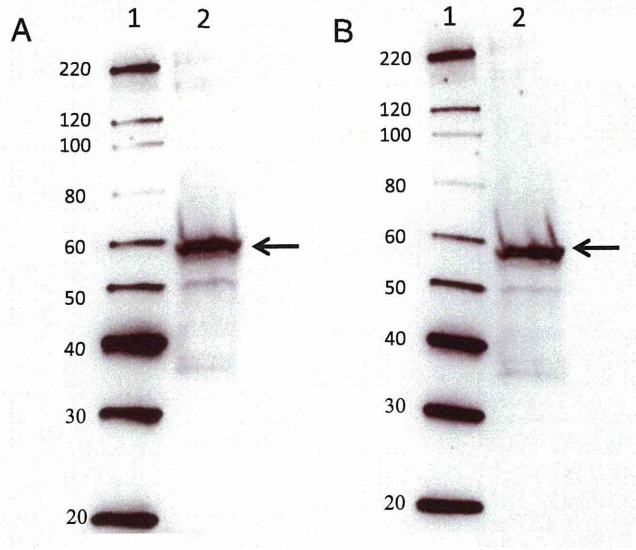

Fig. 5 Western blotting for carnitine palmitoyltransferase 1C (CPT1C) using E-19 (A) and N-18 (B) antibodies in U373MG cells. Lane 1: MagicMark™ XP Western Protein Standard (Life Technologies, Waltham, MA, USA). Lane 2: The arrow indicates the band for CPT1C. The band pattern detected by E-19 (A) is almost identical to that detected by N-18 (B).

21 gliomas with IDH1R132H mutation (100%) and 16 gliomas without the mutation (80%). CPT1C was mainly localized to the nuclei of glioma cells (Figs 6C, 7C, 8C, 9C). p-ACC1 was expressed in 20 gliomas with IDH1R132H mutation (95%) and 19 gliomas without the mutation (95%). p-ACC1 was mainly localized to the nuclei of glioma cells (Figs 6D, 7D, 8D, 9D). Thus, most gliomas expressed FASN in the cytoplasm, and CPT1C and p-ACC1 in the nuclei, irrespective of the presence or absence of the IDH1R132H mutation. However, individual tumor cells often showed different immunopositivities for each protein (Fig. 7). Additionally, some glioma tissues were immunonegative for these FA-related proteins (Fig. 10). Unlike for the cultured cells, the anti-ACC1 antibody was not applicable for the paraffin sections probably because of antigen masking.

Table 1 Classification of human diffuse gliomas

IDH1R132H mutation			
Negative	Number	Positive	Number
Grade 4		Grade 4	
GBM	18	GBM	4
Grade 3		Grade 3	
AA	2	AA	1
		AOL	6
		AOA	3
		Grade 2	
		DA	3
		OL	2
		OA	2
Total	20		21

Forty-one gliomas are composed of 21 cases with the IDH1R132H mutation and 20 cases without the IDH1 mutation. Glioblastoma (GBM), anaplastic astrocytoma (AA), anaplastic oligodendroglioma (AOL), anaplastic oligoastrocytoma (AOA), diffuse astrocytoma (DA), oligodendroglioma (OL) and oligoastrocytoma (OA).

Expression of FA metabolism-related proteins in neuronal and mixed neuronal–glial tumor cells

Because non-neoplastic neurons expressed FASN, CPT1C and p-ACC1, we examined the expression of these proteins in neuronal and mixed neuronal–glial tumors (two gangliogliomas and three central neurocytomas) (Fig. 11). In gangliogliomas, FASN was mainly expressed in the perikarya of ganglion cells and the cytoplasm of glioma cells (Fig. 11B). CPT1C and p-ACC1 (Fig. 11C, D) were expressed in the nuclei of both components. CPT1C was also expressed in the perikarya of ganglion cells. Neurocytomas showed similar staining patterns for these proteins (data not shown).

DISCUSSION

ACC catalyzes the carboxylation of acetyl-CoA into malonyl-CoA.[7] ACC is inactivated upon phosphorylation by AMP-activated protein kinase (AMPK).[7] Thus, malonyl-CoA and ACC facilitate FA synthesis using FASN, while they inhibit β-oxidation using CPT1. We

Table 2 Semiquantitative analysis of fatty acid metabolism-related protein immunostaining in human glioma tissues

IDH1R132H	Number	FASN (%)	CPT1C (%)	p-ACC1 (%)	Grading	Number	FASN (%)	CPT1c (%)	p-ACC1 (%)
Negative (ne)	20	18 (90)	16 (80)	19 (95)	GBM (ne + po)	22	20 (91)	19 (86)	21 (95)
Positive (po)	21	21 (100)	21 (100)	20 (95)	GBM (ne)	18	16 (89)	15 (83)	17 (94)
Total	41	39 (95)	37 (90)	39 (95)	Grade 3 (ne + po)	12	12 (100)	12 (100)	11 (92)
					Grade 3 (po)	10	10 (100)	10 (100)	9 (90)
					Grade 2 (po)	7	7 (100)	7 (100)	7 (100)

Positive (po) indicates the presence of the IDH1R132H mutation and negative (ne) indicates the absence of this IDH1 mutation. GBM, glioblastoma; FASN, fatty acid synthase; CPT1C, carnitine palmitoyltransferase 1C; p-ACC1, phosphorylated acetyl-CoA carboxylase 1.

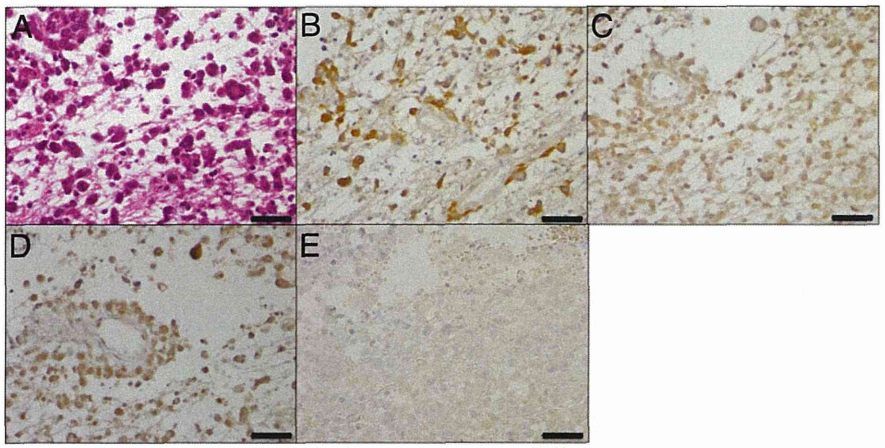

Fig. 6 Expression of fatty acid synthase (FASN), carnitine palmitoyltransferase 1C (CPT1C) and phosphorylated acetyl-CoA carboxylase 1 (p-ACC1) in a glioblastoma specimen without the IDH1R132H mutation. (A) HE staining. FASN is localized to the cytoplasm (B), while CPT1C (C) and p-ACC1 (D) are found in the nucleus. Tumor cells are totally negative for IDH1R132H mutation (E). Bar: 50 μm.

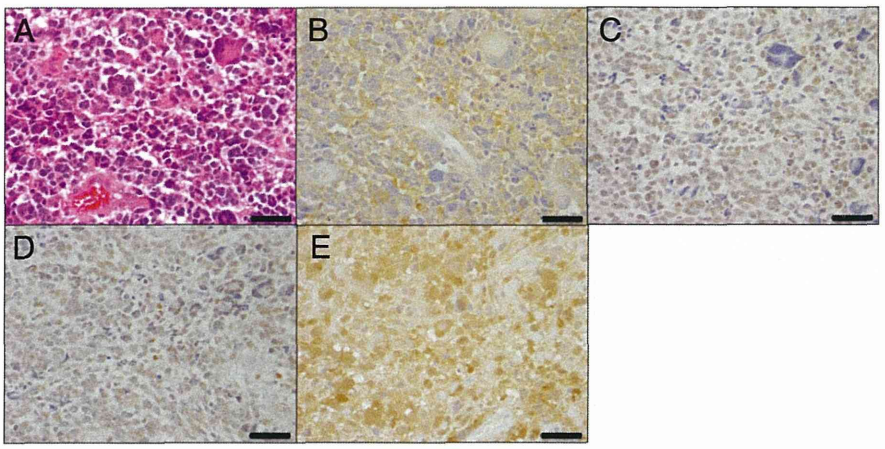

Fig. 7 Expression of fatty acid synthase (FASN), carnitine palmitoyltransferase 1C (CPT1C) and phosphorylated acetyl-CoA carboxylase 1 (p-ACC1) in a glioblastoma specimen with the IDH1R132H mutation. (A) HE staining. FASN is localized to the cytoplasm (B), while CPT1C (C) and p-ACC1 (D) are found in the nucleus. Multinucleated tumor cells are immunonegative for these antibodies. Most tumor cells show IDH1R132H mutation (E). Bar: 50 μm.

showed the differential phosphorylation status of ACC in cellular compartments. Phosphorylated ACC1 in glioma cells was localized in the nuclei in the culture cells and the pathological specimens. Increased expression of FASN has been reported in many tumors including gliomas.[11–13] In meningioma, FASN expression has been implicated in anaplasia. In fact, proliferation of cancer cells was inhibited by suppression of FASN.[4] Hispidulin, a naturally occurring flavone that activates AMPK, has been reported to block proliferation of glioblastoma cells by inhibiting lipogenic enzymes, including ACC and FASN.[14] It has been reported that knockdown of either ATP citrate lyase (ACLY) or FASN in colorectal cancer cells decreases expression of CD44 and inactivates its downstream mediators that regulate cell adhesion, invasion and metastasis.[15] Knockdown of FASN also inhibited angiogenesis in colorectal cancer tissues through downregulation of VEGF.[16] Moreover, pharmacological inhibition of ACC activity with 5-(tetradecyloxy)-2-furoic acid or CP-640186, or ACC1 knockdown with small short interfering RNA, reduced invadopodia formation and inhibited cellular invasion of tumor cells, including glioblastoma cells.[17] In our study, FASN was constitutively expressed in human diffuse gliomas with and without IDH1R132H mutation, regard-

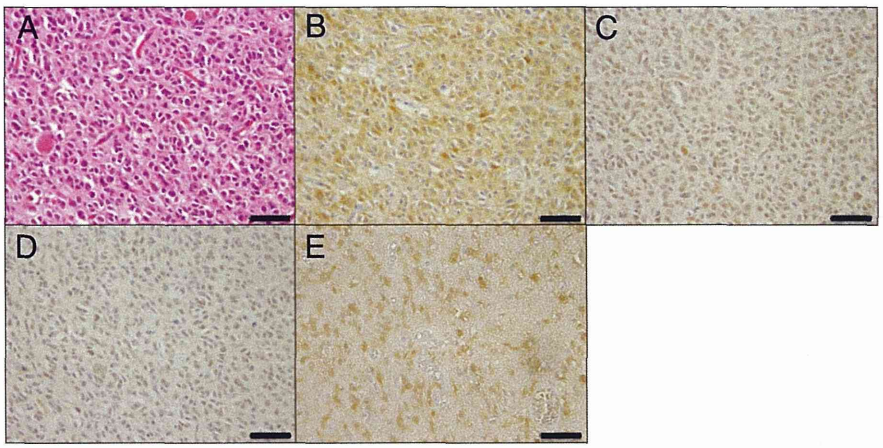

Fig. 8 Expression of fatty acid synthase (FASN), carnitine palmitoyltransferase 1C (CPT1C) and phosphorylated acetyl-CoA carboxylase 1 (p-ACC1) in an oligodendroglioma with the IDH1R132H mutation. (A) HE staining. FASN is localized to the cytoplasm (B), while CPT1C (C) and p-ACC1 (D) are found in the nucleus. All tumor cells show IDH1R132H mutation (E). Bar: 50 μm.

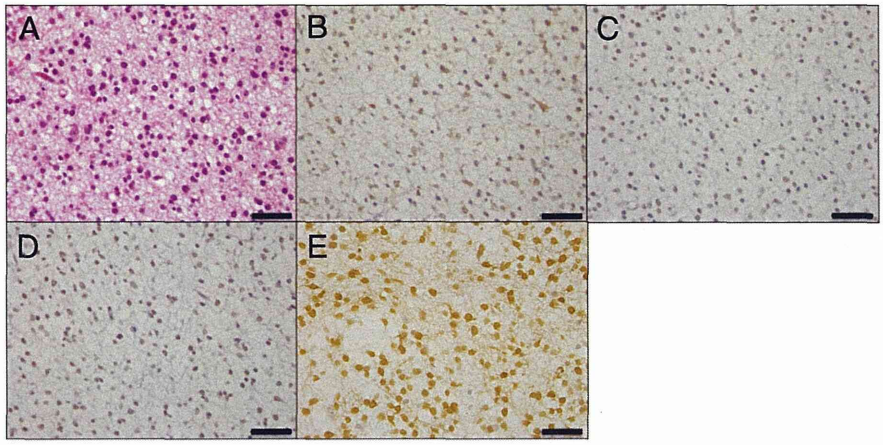

Fig. 9 Expression of fatty acid synthase (FASN), carnitine palmitoyltransferase 1C (CPT1C) and phosphorylated acetyl-CoA carboxylase 1 (p-ACC1) in a diffuse astrocytoma with the IDH1R132H mutation. (A) HE staining. FASN is localized to the cytoplasm (B), while CPT1C (C) and p-ACC1 (D) are found in the nucleus. All tumor cells show IDH1R132H mutation (E). Bar: 50 μm.

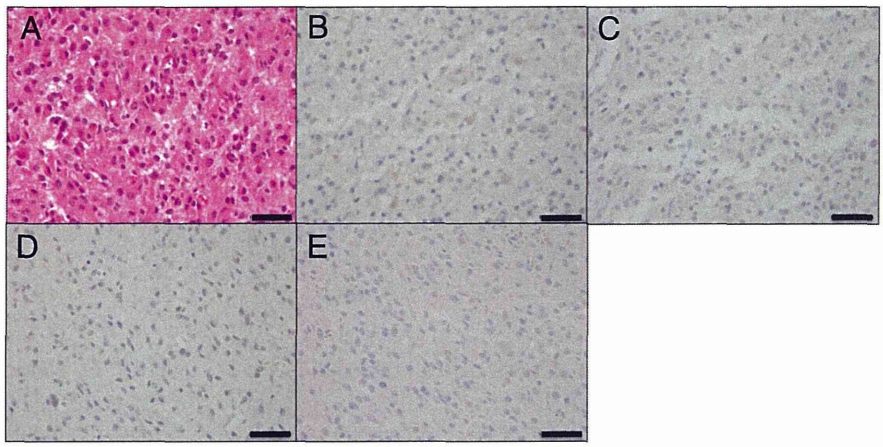

Fig. 10 Expression of fatty acid synthase (FASN), carnitine palmitoyltransferase 1C (CPT1C) and phosphorylated acetyl-CoA carboxylase 1 (p-ACC1) in an anaplastic astrocytoma without the IDH1R132H mutation. (A) HE staining. The tumor cells are immunonegative for CPT1C (C) and p-ACC1 (D) and weakly positive (±) for FASN. Tumor cells are totally negative for IDH1R132H mutation (E). Bar: 50 μm.

less of either histotype or grading. This coincided with nuclear segregation of phosphorylated ACC1, which inhibits lipid synthesis.

CPT1C is a brain-specific isoform of the CPT1 family and is normally expressed in the microsomal fraction of neurons. Although still not fully understood, CPT1C is thought to exist exclusively in the endoplasmic reticulum of neurons and binds malonyl-CoA with the same affinity as CPT1A, but its enzymatic activity is 100 times lower than that of CPT1A and CPT1B.[8,18–20] In this study, we found that CPT1C was expressed in the perikarya of normal neurons; however, in glioma cells, CPT1C was distributed in the cytoplasm and the nuclei. Kim *et al.* have shown the interaction among AMPK, ACC and CPT1

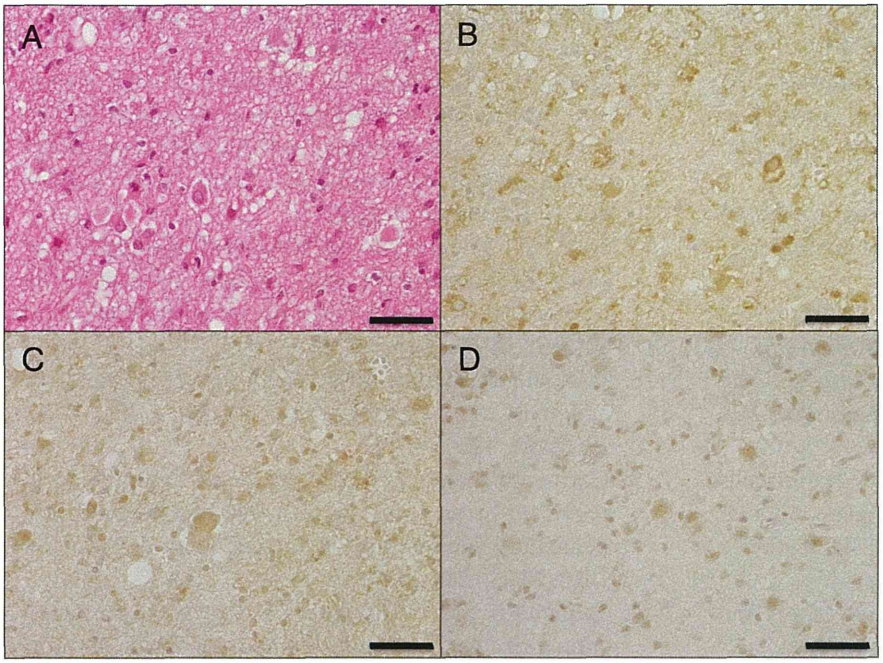

Fig. 11 Expression of fatty acid synthase (FASN), carnitine palmitoyltransferase 1C (CPT1C) and phosphorylated acetyl-CoA carboxylase 1 (p-ACC1) in a ganglioglioma. (A) HE staining. FASN (B) is expressed in the perikarya of ganglion cells and the cytoplasm of glial tumor cells. CPT1C (C) and p-ACC1 (D) are expressed in the nuclei of both components. Additionally, CPT1C is expressed in the perikarya of ganglion cells. Bar: 50 μm.

with the use of clozapine that phosphorylates AMPK (p-AMPK).[21] They reported that intraperitoneal clozapine injection in the rat resulted in increased nuclear expression of p-AMPK and p-ACC in neurons in the frontal cortex, followed by increased activity of CPT1C. In addition, they suggested that the activity of CPT1C was inhibited by unphosphorylated ACC. Similarly, p-ACC1 in glioma cells was strictly localized in the nuclei. CPT1C expression in the endoplasmic reticulum might be suppressed by ACC, while the nuclear translocation of CPT1C might be promoted by p-ACC.

Functions of CPT1C have been reported in several studies. While CPT1C has been shown to play little role in β-oxidation, its relation to ω-oxidation of VLFAs has been suggested.[9,22,23] Carrasco *et al.* have shown that CPT1C regulates the ceramide level independent of *de novo* ceramide synthesis.[19] CPT1C regulates dendritic spine maturation by increasing the ceramide level in the hippocampal neurons. CPT1C is thought to control food intake and energy homeostasis.[18,22,24–27] CPT1C knockout mice showed decreased appetite and body weight compared with control mice; however, the knockout mice are highly susceptible to obesity when fed with a high-fat diet.[26,27]

With regard to tumors, the mRNA level of CPT1C is increased in certain types of tumors, including gliomas and medulloblastomas.[5] Zaugg *et al.* reported that carcinoma cells overexpressing CPT1C showed increased FA oxidation and ATP production.[28] This study also revealed that CPT1C was induced by hypoxia or glucose deprivation and its expression was regulated by AMPKα. Thus, in carcinoma cells, CPT1C might be regulated by AMPKα in a similar fashion to other CPT1 isoforms.[21,28,29] In addition, Lee *et al.* reported that the 5-oxoproline level was decreased and that the level of the oxidized form of glutathione (GSSG) was increased in CPT1C knockout mice, suggesting that CPT1C is associated with resistance to metabolic and oxidative stresses in cancer cells.[23] The elevated expression of CTP1C in gliomas may be advantageous to their survival and growth.

Whereas Western blot analysis confirmed the specificity of the anti-FASN antibody we used in the present study, the two antibodies for different epitopes of CPT1C both detected a band with a molecular weight around 60 kDa, which is smaller than that previously reported.[8] These findings suggest the existence of an unknown splice variant or posttranslational truncation of CPT1C. This isoform might be associated with its nuclear translation in tumor cells.

We observed that various glioma cells coexpressed CPT1C and FASN; however, individual glioma cells showed different immunopositivities for each FA metabolism-related protein even in the same tissue samples. This indicates that a glioma tissue is composed of heterogeneous groups of cells with different FA metabolic statuses, which might contribute to their ability to selectively survive during tumor progression.

ACKNOWLEDGMENTS

We thank Ms. Aya Sakai and Ms. Sachiko Koyama, Department of Neuropathology, Kyushu University, for their excellent technical assistance. This work was supported by JSPS KAKENHI Grant Number 23500429 (SOS).

REFERENCES

1. Vander Heiden MG, Cantley LC, Thompson CB. Understanding the Warburg effect: the metabolic requirements of cell proliferation. *Science* 2009; **324**: 1029–1033.
2. Parsons DW, Jones S, Zhang X *et al.* An integrated genomic analysis of human glioblastoma multiforme. *Science* 2008; **321**: 1807–1812.
3. Yan H, Parsons DW, Jin G *et al.* IDH1 and IDH2 mutations in gliomas. *N Engl J Med* 2009; **360**: 765–773.
4. Menendez JA, Lupu R. Fatty acid synthase and the lipogenic phenotype in cancer pathogenesis. *Nat Rev Cancer* 2007; **7**: 763–777.
5. Reilly PT, Mak TW. Molecular pathways: tumor cells Co-opt the brain-specific metabolism gene CPT1C to promote survival. *Clin Cancer Res* 2012; **18**: 5850–5855.
6. Wolfgang MJ, Hypothalamic LMD. malonyl-CoA and CPT1c in the treatment of obesity. *FEBS Journal* 2011; **278**: 552–558.
7. Schreurs M, Kuipers F, van der Leij FR. Regulatory enzymes of mitochondrial beta-oxidation as targets for treatment of the metabolic syndrome. *Obes Rev* 2010; **11**: 380–388.
8. Sierra AY, Gratacos E, Carrasco P *et al.* CPT1c is localized in endoplasmic reticulum of neurons and has carnitine palmitoyltransferase activity. *J Biol Chem* 2008; **283**: 6878–6885.
9. Reamy AA, Wolfgang MJ. Carnitine palmitoyltransferase-1c gain-of-function in the brain results in postnatal microencephaly. *J Neurochem* 2011; **118**: 388–398.
10. David NL, Cavenee WK *et al. World Health Organization Classification of Tumours of the Nervous System*, 4th edn. Lyon: IARC/WHO, 2007.
11. Makino K, Nakamura H, Hide T *et al.* Usefulness of immunohistochemical expression analysis of metabolic-related molecules to differentiate between intracranial neoplastic and non-neoplastic lesions. *Brain Tumor Pathol* 2013; **30**: 144–150.
12. Haase D, Schmidl S, Ewald C *et al.* Fatty acid synthase as a novel target for meningioma therapy. *Neuro Oncol* 2010; **12**: 844–854.
13. Makino K, Nakamura H, Hide T *et al.* Fatty acid synthase is a predictive marker for aggressiveness in meningiomas. *J Neurooncol* 2012; **109**: 399–404.
14. Lin YC, Hung CM, Tsai JC *et al.* Hispidulin potently inhibits human glioblastoma multiforme cells through activation of AMP-activated protein kinase (AMPK). *J Agric Food Chem* 2010; **58**: 9511–9517.
15. Zaytseva YY, Rychahou PG, Gulhati P *et al.* Inhibition of fatty acid synthase attenuates CD44-associated signaling and reduces metastasis in colorectal cancer. *Cancer Res* 2012; **72**: 1504–1517.
16. Zaytseva YY, Elliott VA, Rychahou P *et al.* Cancer cell-associated fatty acid synthase activates endothelial cells and promotes angiogenesis in colorectal cancer. *Carcinogenesis* 2014; published online 2014 March 7. doi: 10.1093/carcin/bgu042.
17. Scott KE, Wheeler FB, Davis AL *et al.* Metabolic regulation of invadopodia and invasion by acetyl-CoA carboxylase 1 and de novo lipogenesis. *PLoS ONE* 2012; **7**: e29761.
18. Wolfgang MJ, Lane MD. The role of hypothalamic malonyl-CoA in energy homeostasis. *J Biol Chem* 2006; **281**: 37265–37269.
19. Carrasco P, Sahun I, McDonald J *et al.* Ceramide levels regulated by carnitine palmitoyltransferase 1C control dendritic spine maturation and cognition. *J Biol Chem* 2012; **287**: 21224–21232.
20. Samanta S, Situ AJ, Ulmer TS. Structural characterization of the regulatory domain of brain carnitine palmitoyltransferase 1. *Biopolymers* 2014; **101**: 398–405. doi: 10.1002/bip.22396.
21. Kim MK, Kim SH, Yu HS *et al.* The effect of clozapine on the AMPK-ACC-CPT1 pathway in the rat frontal cortex. *Int J Neuropsychopharmacol* 2012; **15**: 907–917.
22. Wolfgang MJ, Cha SH, Millington DS *et al.* Brain-specific carnitine palmitoyl-transferase-1c: role in CNS fatty acid metabolism, food intake, and body weight. *J Neurochem* 2008; **105**: 1550–1559.
23. Lee J, Wolfgang MJ. Metabolomic profiling reveals a role for CPT1c in neuronal oxidative metabolism. *Bmc Biochem* 2012; **25**: 13–23. doi: 10.1186/1471-2091-13-23.
24. Wolfgang MJ, Kurama T, Dai Y *et al.* The brain-specific carnitine palmitoyltransferase-1c regulates energy homeostasis. *Proc Natl Acad Sci USA* 2006; **103**: 7282–7287.
25. Dai Y, Wolfgang MJ, Cha SH, Lane MD. Localization and effect of ectopic expression of CPT1c in CNS feeding centers. *Biochem Biophys Res Commun* 2007; **359**: 469–474.
26. Lane MD, Wolfgang M, Cha SH, Dai Y. Regulation of food intake and energy expenditure by hypothalamic malonyl-CoA. *Int J Obes (Lond)* 2008; **32** (Suppl 4): S49–S54.
27. Gao XF, Chen W, Kong XP *et al.* Enhanced susceptibility of Cpt1c knockout mice to glucose intolerance induced by a high-fat diet involves elevated hepatic gluconeogenesis and decreased skeletal muscle glucose uptake. *Diabetologia* 2009; **52**: 912–920.
28. Zaugg K, Yao Y, Reilly PT *et al.* Carnitine palmitoyltransferase 1C promotes cell survival and tumor growth under conditions of metabolic stress. *Genes Dev* 2011; **25**: 1041–1051.

29. Lohse I, Reilly P, Zaugg K. The CPT1C 5'UTR contains a repressing upstream open reading frame that is regulated by cellular energy availability and AMPK. *PLoS ONE* 2011; **6**: e21486.

SUPPORTING INFORMATION

Additional Supporting Information may be found in the online version of this article at the publisher's web-site:

Table S1 Semiquantitative analysis of the results of immunostaining for FA metabolism-related proteins in human glioma tissues without the IDH1R132H mutation.

Table S2 Semiquantitative analysis of the results of FASN immunostaining in human glioma tissues with the IDH1R132H mutation.

Table S3 Semiquantitative analysis of the results of CPT1c immunostaining in human glioma tissues with the IDH1R132H mutation.

Table S4 Semiquantitative analysis of the results of p-ACC1 immunostaining in human glioma tissues with the IDH1R132H mutation.

NEUROPATHOLOGY

Neuropathology 2015; **35**, 37–43 doi:10.1111/neup.12153

Original Article

Loss of hnRNPA1 in ALS spinal cord motor neurons with TDP-43-positive inclusions

Hiroyuki Honda,[1] Hideomi Hamasaki,[1] Tomihiro Wakamiya,[1] Sachiko Koyama,[1] Satoshi O. Suzuki,[1] Naoki Fujii[2] and Toru Iwaki[1]

[1]Department of Neuropathology, Neurological Institute, Graduate School of Medical Sciences, Kyushu University, and [2]Department of Neurology, Neuro-Muscular Center, National Omuta Hospital, Fukuoka, Japan

Amyotrophic lateral sclerosis (ALS) is a fatal neurodegenerative disease characterized by loss of motor neurons and appearance of skein-like inclusions. The inclusions are composed of trans-activation response (TAR) DNA-binding protein 43 (TDP-43), a member of the heterogeneous nuclear ribonucleoprotein (hnRNP) family. hnRNPA1 and hnRNPA2/B1 are hnRNPs that interact with the C-terminus of TDP-43. Using immunohistochemistry, we investigated the association between TDP-43 and hnRNPA1 in ALS spinal motor neurons. We examined spinal cords of seven ALS cases and six muscular dystrophy cases (used as controls) for the presence of TDP-43 and hnRNPA1 protein. In the control cases, hnRNPA1 immunoreactivity in motor neurons was intense in the nucleus and weak in the cytoplasm where it showed a fine granular appearance. In the ALS cases, hnRNPA1 immunoreactivity in motor neurons was reduced in the nuclei of neurons with skein-like inclusions but was not detected in the skein-like inclusions. The marked loss of hnRNPA1 in motor neurons with concomitant cytoplasmic aggregation of TDP-43 may represent a severe disturbance of mRNA processing, suggesting a key role in progressive neuronal death in ALS.

Key words: amyotrophic lateral sclerosis, hnRNP, hnRNPA1, motor neuron, TDP-43.

INTRODUCTION

Amyotrophic lateral sclerosis (ALS) is a degenerative and fatal motor neuron disease. The primary neuropathological feature of ALS is a selective loss of motor neurons and the presence of skein-like inclusions (SLIs) in residual motor neurons. Trans-activation response (TAR) DNA-binding protein of 43 kDa (TDP-43) is an RNA-binding protein and the principle protein component of SLIs in affected motor neurons.[1,2] Missense mutations in *TARDBP* have been reported in both sporadic ALS and familial ALS, implying that abnormal TDP-43 protein may cause neurodegeneration.[3–5] The major protein domains of TDP-43 include two RNA-binding motifs that mediate binding to transcripts, and a C-terminal glycine-rich region that is required for interaction with other RNA-binding proteins, such as heterogeneous nuclear ribonucleoproteins (hnRNPs), including hnRNPA1 and hnRNP A2/B1.[6] hnRNPA1 is a key molecule in mRNA metabolism, microRNA biogenesis and DNA-related functions.[7] hnRNPA1 has been reported to contribute to several neurodegenerative diseases, including Alzheimer disease,[8,9] ALS,[10,11] frontotemporal lobar degeneration (FTLD),[12] spinal muscular atrophy,[13] multiple sclerosis,[14,15] and HTLV-I-associated myelopathy/tropical spastic paraparesis.[16] The C-terminal of hnRNPA1 binds to the C-terminal of TDP-43 and the resultant complex regulates splicing inhibitory activity.[17] In this study, we investigated the association between TDP-43 and hnRNPA1 in motor neurons of sporadic ALS cases, using immunohistochemical techniques.

MATERIALS AND METHODS

Post mortem spinal cord tissue

Using the revised El Escorial criteria,[18] seven patients were diagnosed with ALS at the National Omuta Hospital, Fukuoka, Japan. All diagnoses were made by the same neurologist with a sufficient carrier for diagnosis of neurodegenerative disorders. The patients died between 2007 and 2013 and general autopsies were carried out.

Correspondence: Toru Iwaki, MD, PhD, Department of Neuropathology, Graduate School of Medical Sciences, Kyushu University, 3-1-1 Maidashi, Higashi-ku, Fukuoka 812-8582, Japan. Email: iwaki@np.med.kyushu-u.ac.jp

Received 25 June 2014; revised and accepted 11 August 2014; published online 22 October 2014.

Table 1 Profiles of ALS cases and control cases

Case	Age at death	Sex	PMI (h)	Brain weight (g)	Diagnosis
1	67	F	31	1230	ALS
2	73	M	17	1290	ALS
3	77	F	12	1250	ALS
4	80	F	10	1080	ALS
5	80	M	4	1235	ALS
6	80	F	24	1100	ALS
7	88	F	9	1170	ALS
8	14	M	6	1370	DMD
9	17	M	3	1400	DMD
10	20	M	22	1430	DMD
11	56	M	20	1200	MyD
12	60	F	13	1170	MyD
13	61	M	14	1190	MyD

ALS, amyotrophic lateral sclerosis; DMD, Duchenne muscular dystrophy; F, female; M, male; MyD, myotonic dystrophy; PMI, post mortem interval.

Control cases included three cases of Duchenne muscular dystrophy (DMD) and three cases of myotonic dystrophy (MyD). Multiple 6-μm-thick sections of buffered formalin-fixed, paraffin-embedded spinal cord specimens were stained with HE and KB staining. The details of cases are shown in Table 1.

Immunohistochemistry

Immunohistochemistry was performed using primary antibodies against phosphorylated TDP-43 (p-TDP-43; polyclonal, rabbit, 1:5000; Cosmo Bio, Tokyo, Japan), TDP-43 (polyclonal, rabbit, 1:2000; Protein Tech Group Inc., Chicago, IL, USA) and hnRNPA1 (9H10; monoclonal, mouse, 1:1000; abcam, Cambridge, UK). Tissues were pretreated with hydrated autoclaving at 121°C for 10 min for antigen retrieval. The sections were incubated with primary antibodies overnight at 4°C. After rinsing, immunoreaction products were detected by the polymer immunocomplex method using an Envision system (DakoCytomation, Glostrup, Denmark). Immunoreactivity was visualized using 3, 3′-diaminobenzidine (DAB, Dojindo, Kumamoto, Japan), and specimens were lightly counterstained with hematoxylin.

Immunofluorescence

We performed double immunofluorescence labeling using a rabbit polyclonal anti-p-TDP-43 antibody and a mouse monoclonal anti-hnRNPA1 antibody, or a rabbit polyclonal anti-TDP-43 antibody and a mouse monoclonal anti-hnRNPA1 antibody. Alexa 488-labeled anti-mouse IgG (Invitrogen, Carlsbad, CA, USA) and Alexa 546-labeled anti-rabbit IgG (Invitrogen) were used as secondary antibodies. The primary and secondary antibodies were used at a dilution of 1:50. Sections were deparaffinized in xylene and rehydrated in ethanol and then autoclaved in 0.01 mol/L citrate buffer to unmask the epitope. Slides were then incubated with the primary antibodies overnight at 4°C. After rinsing, sections were incubated in the appropriate secondary antibody for 1 h at room temperature and then counterstained with 4′,6-diamidino-2-phenylindole (Invitrogen) and visualized using a Nikon A1R-A1 Confocal Microscope System (Nikon, Tokyo, Japan).

Quantification of motor neurons

We performed immunohistochemistry on serial sections of spinal cords to investigate the intracellular localization of hnRNPA1 and p-TDP-43 or TDP-43 in individual motor neurons. Immunoreactivity for nuclear hnRNPA1was semi-quantitatively scored either as negative, weakly positive or positive signals.

Statistical analysis

We used Chi-square test to compare the number of anterior horn cells in ALS cases with that in control cases using JMP 9.02 software (SAS Institute, Raleigh, NC, USA).

RESULTS

Anterior horn cells and corticospinal tracts were well preserved in control muscular dystrophy subjects. Immunohistochemistry for hnRNPA1 revealed intense immunoreactivity in the nuclei of the majority of cells in the anterior horn and posterior horn (Fig. 1A,B). A small number of anterior horn cells showed a complete loss of nuclear immunoreactivity for hnRNPA1 (Table 2).

We observed a marked decline of nuclear and cytoplasmic hnRNPA1 immunoreactivity in the anterior horn cells of ALS cases (Fig. 1C). However, posterior horn cells maintained nuclear hnRNPA1 immunoreactivity (Fig. 1D). Immunohistochemistry for p-TDP-43 revealed intense immunoreactivity in SLIs in the remaining anterior horn cells in all ALS subjects (Fig. 2A). Forty-four percent of anterior horn cells lost nuclear immunoreactivity for hnRNPA1 (Table 2). The number of motor neurons that lost immunoreactivity for nuclear hnRNPA1 was significantly larger than that of control cases (vs. DMD: $P < 0.001$; vs. MyD: $P < 0.001$). On serial sections (Fig. 2A,B) and double immunofluorescence for p-TDP-43 and hnRNPA1 (Fig. 2C–F), 84.1% (37/44) of motor neurons with SLIs showed a marked decline of nuclear hnRNPA1 immunoreactivity (Table 3). Colocalization of hnRNPA1 and p-TDP-43 in SLIs was not observed (Fig. 2C–F). As shown in Table 3, SLIs were rarely observed in motor neurons that showed intense nuclear hnRNPA1 immunoreactivity (2.3%: 1/44). Including motor neurons with intense and weak nuclear hnRNPA1

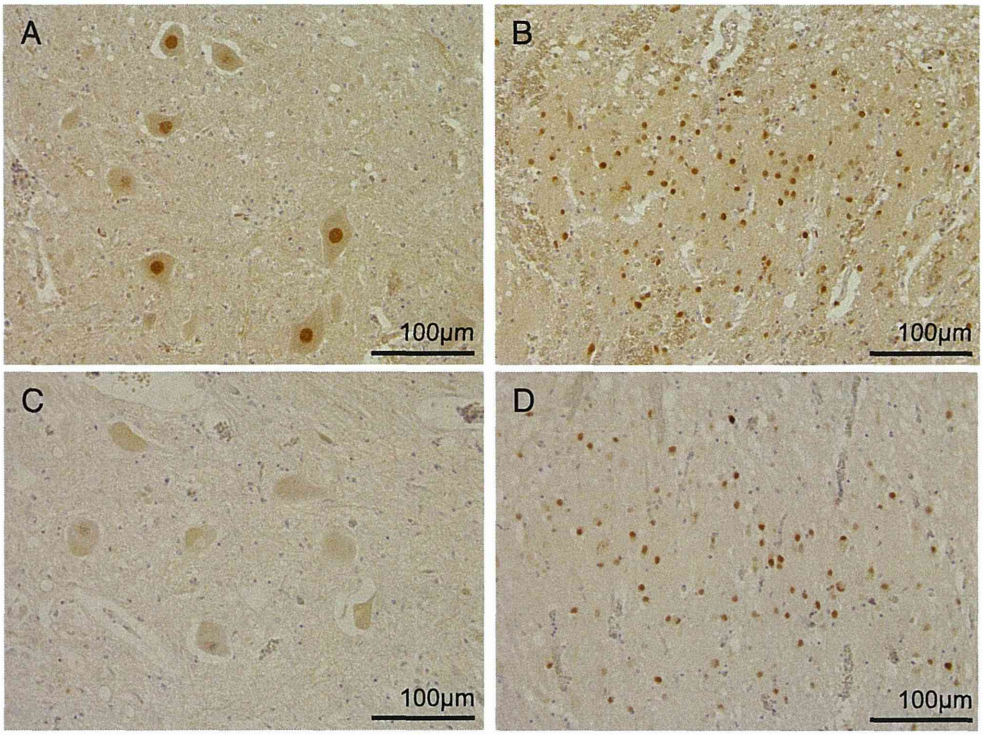

Fig. 1 Expression of heterogeneous nuclear ribonucleoprotein A1 (hnRNPA1) in spinal anterior horn cells and posterior horn cells of the control case (A, B: Case 13) and the ALS case (C, D: Case 2). (A) Immunohistochemistry for hnRNPA1 shows intense nuclear immunoreactivity in the anterior horn cells. Weak granular cytoplasmic hnRNPA1 immunoreactivity is also noted. (B) Almost all posterior horn cells show intense nuclear immunoreactivity. (C) In ALS, a marked decline of immunoreactivity for hnRNPA1 is noted in the nucleus and cytoplasm. (D) Almost all posterior horn cells show intense nuclear immunoreactivity.

Table 2 Nuclear hnRNPA1 immunoreactivity in spinal motor neurons

	ALS ($n = 7$)	DMD ($n = 3$)	MyD ($n = 3$)
Positive	37.6% (41/109)	64.6% (159/246)	59.2% (170/287)
Weakly positive	18.3% (20/109)	18.7% (46/246)	17.4% (50/287)
Negative	44.0% (48/109)	16.7% (41/246)	23.3% (67/287)

ALS, amyotrophic lateral sclerosis; DMD, Duchenne muscular dystrophy; MyD, myotonic dystrophy; hnRNPA1, heterogeneous nuclear ribonucleoprotein A1.

Table 3 Nuclear hnRNPA1 immunoreactivities in spinal motor neurons of ALS

Nuclear hnRNPA1	Neurons with SLI ($n = 44$)	Neurons without SLI ($n = 65$)
Positive	2.3% (1/44)	61.5% (40/65)
Weakly positive	13.6% (6/44)	21.5% (14/65)
Negative	84.1% (37/44)	16.9% (11/65)

ALS, amyotrophic lateral sclerosis; SLI, skein-like inclusion; hnRNPA1, heterogeneous nuclear ribonucleoprotein A1.

immunoreactivities, these neurons showed significantly fewer SLIs than that of neurons without nuclear hnRNPA1 immunoreactivity ($P < 0.001$).

On serial sections of ALS cases with double immunofluorescence for TDP-43 and hnRNPA1, motor neurons with intense nuclear hnRNPA1 immunoreactivity also retained nuclear TDP-43 immunoreactivity (Fig. 3A–D). Among nuclear hnRNPA1-negative motor neurons, nuclear TDP-43-positive neurons were rarely seen (Table 4). Several neurons that were weakly positive for nuclear hnRNPA1 immunoreactivity had SLIs (Fig. 3E–H). The motor neurons that lost nuclear hnRNPA1 immunoreactivity usually had SLIs (Fig. 3I–L).

DISCUSSION

This is the first study concerning hnRNPA1 immunohistochemistry in human spinal cords. We initially investigated cellular distribution of hnRNPA1 in spinal cords of muscular dystrophy cases. Although muscular dystrophy patients presented marked muscular atrophy, spinal motor neurons were well preserved and most motor neurons

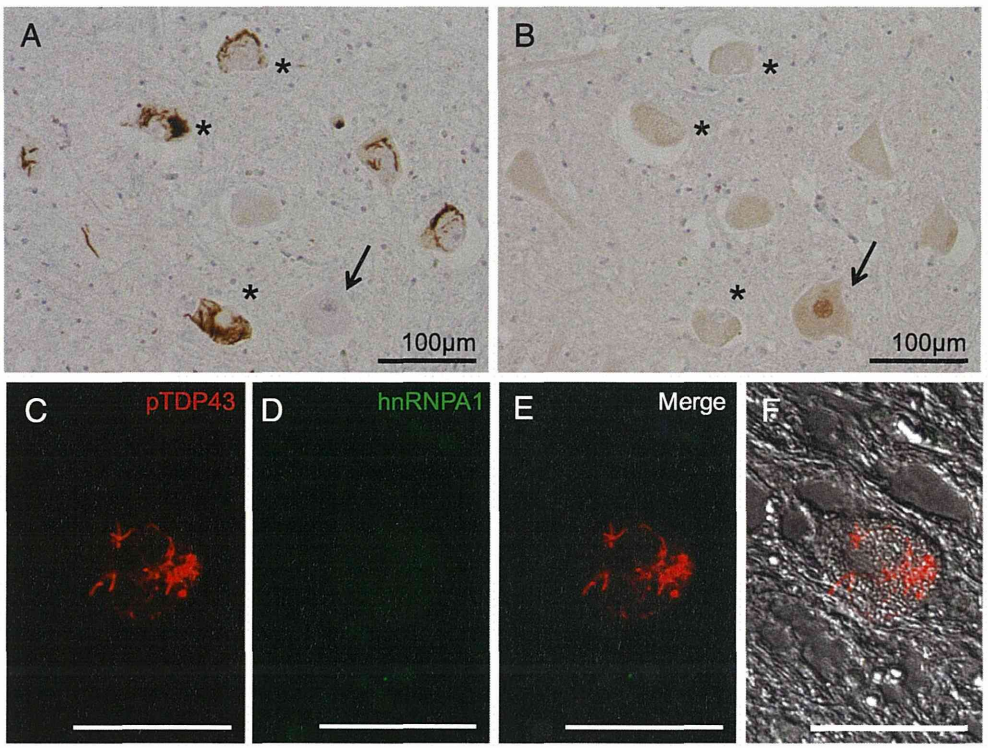

Fig. 2 Immunohistochemistry for p-TDP-43 and heterogeneous nuclear ribonucleoprotein A1 (hnRNPA1) in ALS spinal motor neurons (Case 4). (A, B) Immunohistochemistry for p-TDP-43 (trans-activation response (TAR) DNA-binding protein of 43 kDa) (A) and hnRNPA1 (B) on adjacent sections. Motor neurons with p-TDP-43 positive skein-like inclusions (SLIs) (asterisks in A) show marked decline of nuclear hnRNPA1 immunoreactivity (asterisks in B). The arrow points to a normal-appearing motor neuron, which preserves both intense nuclear and weak cytoplasmic immunoreactivity for hnRNPA1 (B). (C–F) Double immunofluorescence for p-TDP-43 (red) and hnRNPA1 (green). SLI is revealed by anti-p-TDP-43 antibody in the motor neuron, in which nuclear immunoreactivity for hnRNPA1 is completely lost. Differential interference contrast (Nomarski) imaging reveals cytoplasmic localization of p-TDP-43-positive SLI. Scale bars correspond to 50 μm (C–F).

Table 4 Nuclear immunoreactivities of hnRNPA1 and TDP-43 in spinal motor neurons of ALS

	TDP-43 (+)	TDP-43 (–)
hnRNPA1 (+)	32.6% (31/95)	26.3% (25/95)
hnRNPA1 (–)	6.3% (6/95)	34.7% (33/95)

hnRNPA1, heterogeneous nuclear ribonucleoprotein A1; TDP-43, trans-activation response (TAR) DNA-binding protein of 43 kDa.

retained nuclear hnRNPA1 expression. In ALS spinal cords, we frequently observed loss of hnRNPA1 immunoreactivity in motor neurons. We also demonstrated that reduced levels of hnRNPA1 in sporadic ALS motor neurons correlated well with formation of TDP-43-positive inclusions. Indeed, all neurons with SLIs either lost or had weakened nuclear hnRNPA1 immunoreactivity. Our results suggest the involvement of disappearance of nuclear hnRNPA1 in the disease processes of sporadic ALS cases.

hnRNPA1 is a member of the heterogeneous nuclear ribonucleoprotein family that plays a role in mRNA metabolism, microRNA biogenesis, and DNA-related functions.[7] The N-terminal of hnRNPA1 includes two RNA recognition motifs.[19] The C-terminal of the protein has a glycine-rich domain that harbors a prion-like domain.[10] Additionally, the C-terminal is also a binding site for the C-terminal of TDP-43 and the resulting complex regulates splicing inhibitory activity.[17] hnRNPA1 is located mainly in the nucleus, although it can be found in the cytoplasm. The M9 site of hnRNP A1 is responsible for bidirectional shuttling of hnRNPA1 via the nuclear pore complex.[20]

In this study, nuclear hnRNPA1 immunoreactivity was lost or weak in the nucleus of ALS spinal motor neurons. The disappearance of hnRNPA1 in the nuclei of motor neurons implies a dysfunction of mRNA splicing inhibitory activity. Similar to our findings in ALS cases, Neumann *et al.* reported the absence of nuclear hnRNPs in neurons with TDP-43-positive inclusions in affected brain regions in FTLD cases with TDP-43 proteinopathy.[12] Recently, pathogenic mutations in the prion-like domains of *HNRNPA2/B1* and *HNRNPA1* have been found in families with inherited degeneration affecting muscle, brain, motor neurons, and bone (inclusion body myopathy with

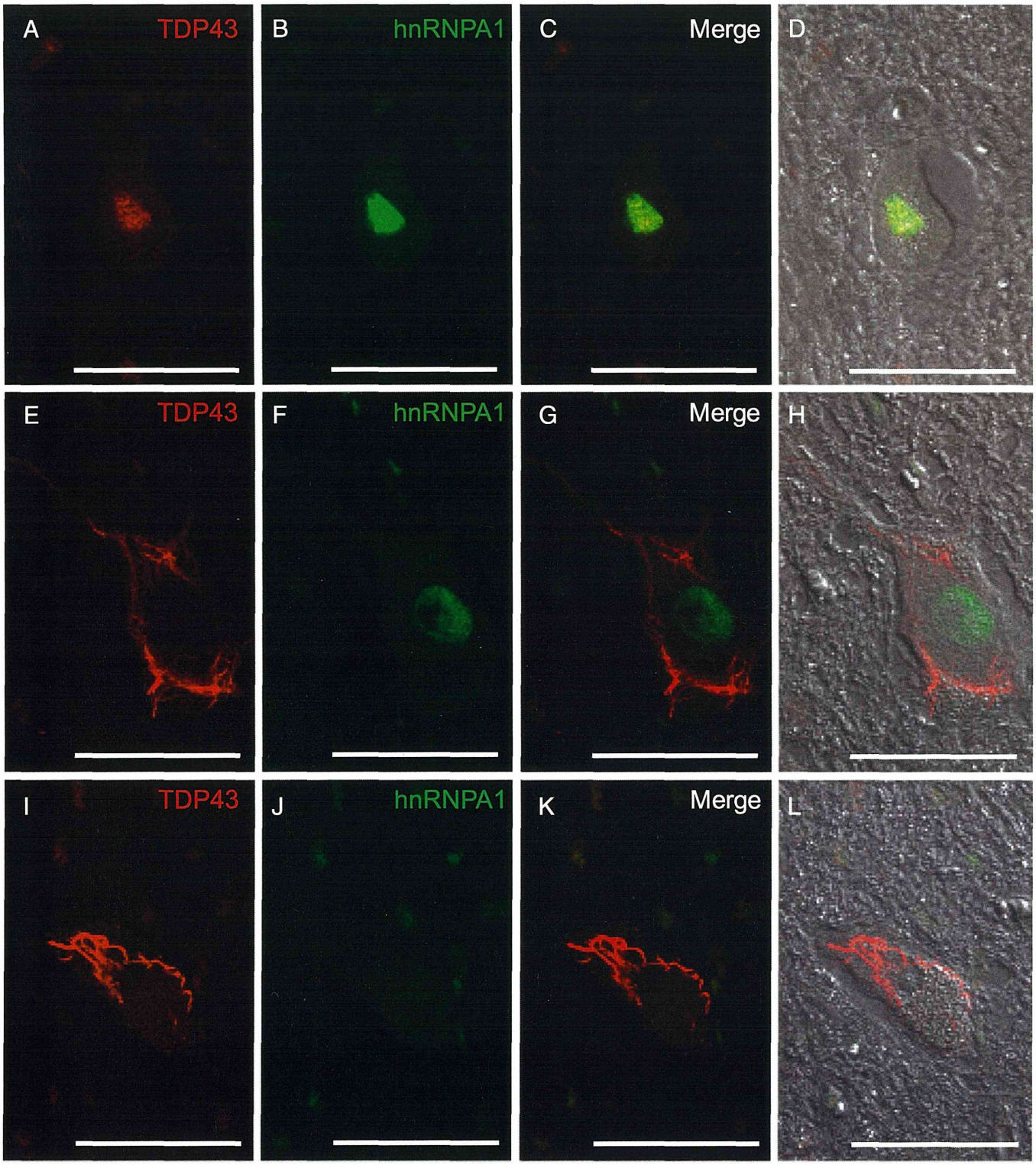

Fig. 3 Double immunofluorescence for TDP-43 (trans-activation response (TAR) DNA-binding protein of 43 kDa) (red) and heterogeneous nuclear ribonucleoprotein A1 (hnRNPA1) (green) in ALS spinal motor neurons (Case 1). In the rightmost column, the merged double immunofluorescence images are further superimposed on the differential interference contrast (Nomarski) images. (A–D) The neuron retains nuclear expression of both TDP-43 and hnRNPA1. (E–H) Only weak hnRNPA1 expression remains in the nucleus of the neuron bearing skein-like inclusions (SLIs). (I–L) The neuron bearing SLI loses both nuclear TDP-43 and hnRNPA1. Scale bars correspond to 50 μm.

Paget disease of bone and/or frontotemporal dementia (IBMPFD2 and IBMPFD3), and in a case of familial ALS (ALS20).[10] In the muscle pathology of the study, TDP-43, hnRNPA2B1 and hnRNPA1 were often cleared from the nuclei of the atrophic muscle fibers, and they often showed partial colocalization in the cytoplasm. In our study, although nuclear hnRNPA1 immunoreactivity in ALS spinal motor neurons was lost or weakened, colocalization of hnRNPA1 and TDP-43 in SLIs was not observed. A subsequent genetic study including 135 familial ALS and 1084 sporadic ALS did not identify any mutations in the prion-like domain of *HNRNPA1* and *HNRNPA2/B1*, thus the mutations may be quite rare in both familial and sporadic ALS.[21]

hnRNPA1 has been reported to have many functions. Reduced nuclear hnRNPA1 disturb mRNA splicing, mRNA stability related to TDP-43, and microRNA biogenesis. Recently, it was reported that TDP-43 regulates its mRNA levels.[22] Therefore, reduced nuclear levels of hnRNPA1 might influence the abnormal distribution of TDP-43. hnRNPA1 also regulates Drosha-mediated miRNA processing.[7] We propose hnRNPA1 might be associated with a variety of pathogeneses and symptoms of ALS. Our results suggest the involvement of abnormal RNA metabolism in the pathogenesis of ALS.

ACKNOWLEDGMENTS

This study was supported in part by a Grant-in-Aid for Scientific Research (B) (No. 26290017) from the Japan Society for the Promotion of Science (JSPS).

REFERENCES

1. Neumann M, Sampathu DM, Kwong LK *et al.* Ubiquitinated TDP-43 in frontotemporal lobar degeneration and amyotrophic lateral sclerosis. *Science* 2006; **314**: 130–133.
2. Arai T, Hasegawa M, Akiyama H *et al.* TDP-43 is a component of ubiquitin-positive tau-negative inclusions in frontotemporal lobar degeneration and amyotrophic lateral sclerosis. *Biochem Biophys Res Commun* 2006; **351**: 602–611.
3. Van Deerlin VM, Leverenz JB, Bekris LM *et al.* TARDBP mutations in amyotrophic lateral sclerosis with TDP-43 neuropathology: a genetic and histopathological analysis. *Lancet Neurol* 2008; **7**: 409–416.
4. Sreedharan J, Blair IP, Tripathi VB *et al.* TDP-43 mutations in familial and sporadic amyotrophic lateral sclerosis. *Science* 2008; **319**: 1668–1672.
5. Kabashi E, Valdmanis PN, Dion P *et al.* TARDBP mutations in individuals with sporadic and familial amyotrophic lateral sclerosis. *Nat Genet* 2008; **40**: 572–574.
6. King OD, Gitler AD, Shorter J. The tip of the iceberg: RNA-binding proteins with prion-like domains in neurodegenerative disease. *Brain Res* 2012; **1462**: 61–80.
7. Bekenstein U, Soreq H. Heterogeneous nuclear ribonucleoprotein A1 in health and neurodegenerative disease: from structural insights to post-transcriptional regulatory roles. *Mol Cell Neurosci* 2013; **56**: 436–446.
8. Donev R, Newall A, Thome J, Sheer D. A role for SC35 and hnRNPA1 in the determination of amyloid precursor protein isoforms. *Mol Psychiatry* 2007; **12**: 681–690.
9. Berson A, Barbash S, Shaltiel G *et al.* Cholinergic-associated loss of hnRNP-A/B in Alzheimer's disease impairs cortical splicing and cognitive function in mice. *EMBO Mol Med* 2012; **4**: 730–742.
10. Kim HJ, Kim NC, Wang YD *et al.* Mutations in prion-like domains in hnRNPA2B1 and hnRNPA1 cause multisystem proteinopathy and ALS. *Nature* 2013; **495**: 467–473.
11. Ayala YM, Pantano S, D'Ambrogio A *et al.* Human, Drosophila, and C. elegans TDP43: nucleic acid binding properties and splicing regulatory function. *J Mol Biol* 2005; **348**: 575–588.
12. Neumann M, Igaz LM, Kwong LK *et al.* Absence of heterogeneous nuclear ribonucleoproteins and survival motor neuron protein in TDP-43 positive inclusions in frontotemporal lobar degeneration. *Acta Neuropathol* 2007; **113**: 543–548.
13. Kashima T, Rao N, David CJ, Manley JL. hnRNP A1 functions with specificity in repression of SMN2 exon 7 splicing. *Hum Mol Genet* 2007; **16**: 3149–3159.
14. Sueoka E, Yukitake M, Iwanaga K, Sueoka N, Aihara T, Kuroda Y. Autoantibodies against heterogeneous nuclear ribonucleoprotein B1 in CSF of MS patients. *Ann Neurol* 2004; **56**: 778–786.
15. Lee S, Xu L, Shin Y *et al.* A potential link between autoimmunity and neurodegeneration in immune-mediated neurological disease. *J Neuroimmunol* 2011; **235**: 56–69.
16. Lee SM, Dunnavant FD, Jang H, Zunt J, Levin MC. Autoantibodies that recognize functional domains of hnRNPA1 implicate molecular mimicry in the pathogenesis of neurological disease. *Neurosci Lett* 2006; **401**: 188–193.
17. Buratti E, Brindisi A, Giombi M, Tisminetzky S, Ayala YM, Baralle FE. TDP-43 binds heterogeneous nuclear ribonucleoprotein A/B through its C-terminal tail: an important region for the inhibition of cystic fibrosis transmembrane conductance regulator exon 9 splicing. *J Biol Chem* 2005; **280**: 37572–37584.
18. Brooks BR. El Escorial World Federation of Neurology criteria for the diagnosis of amyotrophic lateral

sclerosis. Subcommittee on Motor Neuron Diseases/ Amyotrophic Lateral Sclerosis of the World Federation of Neurology Research Group on Neuromuscular Diseases and the El Escorial "Clinical limits of amyotrophic lateral sclerosis" workshop contributors. *J Neurol Sci* 1994; **124** (Suppl): 96–107.
19. Mayeda A, Munroe SH, Xu RM, Krainer AR. Distinct functions of the closely related tandem RNA-recognition motifs of hnRNP A1. *RNA* 1998; **4**: 1111–1123.
20. Siomi H, Dreyfuss G. A nuclear localization domain in the hnRNP A1 protein. *J Cell Biol* 1995; **129**: 551–560.
21. Seelen M, Visser AE, Overste DJ *et al.* No mutations in hnRNPA1 and hnRNPA2B1 in Dutch patients with amyotrophic lateral sclerosis, frontotemporal dementia, and inclusion body myopathy. *Neurobiol Aging* 2014; **35**: 1956e9–1956.e11.
22. Ayala YM, De Conti L, Avendano-Vazquez SE *et al.* TDP-43 regulates its mRNA levels through a negative feedback loop. *EMBO J* 2011; **30**: 277–288.

A Case of Late-Onset Bipolar Disorder With Severely Abnormal Behavior and Neuroimaging Observations Very Similar to Those of Frontotemporal Dementia

To the Editor: Frontotemporal dementia (FTD) is mainly characterized by neuropsychiatric symptoms, usually preceding cognitive impairment, and an early impairment of executive functions, with relatively preserved memory and visuospatial skills.[1] There have thus been some case reports of FTD that is initially diagnosed as schizophrenia or bipolar disorders (BP).[2] We herein report a case of late-onset BP that was initially diagnosed as major depressive disorder and was temporarily diagnosed as FTD because of severely abnormal behaviors and neuroimaging observations that were very similar to those of FTD.

Case Report

The patient was a 52-year-old-man. There was no definite family or past history of mental or neurological diseases. At 42 years of age, he began to show depressive symptoms, including depressive mood and psychomotor retardation. At age 46, he gradually began to show hypomanic symptoms, including hyperactivity and hypersexual talk. He appeared stark naked in an orthopedic hospital and was thus admitted to our hospital at age 47. He sometimes stripped himself to the waist and masturbated in front of others. Valproate (800 mg/day) was immediately prescribed, instead of clomipramine (225 mg/day). Thereafter, his abnormal behaviors were gradually ameliorated; however, he became apathetic and had difficulty in doing his daily activities. Medical examinations, including complete blood count, liver, renal and thyroid function tests, and electroencephalography showed no definite abnormalities. Neuroimaging observations (SPECT) showed predominant frontal hypoperfusion, as well as predominant frontal brain atrophy shown by MRI. A Wisconsin Card-Sorting Test also demonstrated frontal lobe hypofunction. He was thus diagnosed with FTD. However, lithium (600 mg/day) was prescribed instead of valproate because of the possible diagnosis of bipolar disorder. Thereafter, his apathetic symptoms were gradually ameliorated, and he was discharged from our hospital about 22 months after the admission. The abnormalities shown by neuroimaging studies described above were ameliorated after the lithium treatment for BP for about 2 years. He has been euthymic for about 4 years, until the present time.

Discussion

Woolley et al. demonstrated that patients with FTD were more likely to initially present to a psychiatrist than to a neurologist and often receive erroneous psychiatric diagnoses before FTD was correctly diagnosed.[2,3] On the contrary, in the present case, the diagnosis of FTD was temporarily made because of severely abnormal behaviors and neuroimaging observations. To the best of our knowledge, there have been no reports describing late-onset BP preceding the diagnosis of FTD. Ng et al. suggested that the clinician should keep bipolar spectrum disorders in the differential diagnosis of late-onset affective dysregulation in the setting of dementia.[4] Mendez et al. have demonstrated that consensus criteria and neuropsychological measures lacked sensitivity for FTD and that clinical diagnosis of FTD needs to combine neuropsychiatric features with SPECT or PET findings.[5] We clinicians should bear the present case in mind and diagnose carefully in the clinical setting of dementia.

Akira Monji, M.D.
Keisuke Motomura, M.D.
Yoshito Mizoguchi, M.D.
Tomoyuki Ohara, M.D.
Shingo Baba, M.D.
Takashi Yoshiura, M.D.
Shigenobu Kanba, M.D.
Dept. of Psychiatry, Faculty of Medicine, Saga University, Nabeshima 5-1-1, Saga-City, Japan
Dept. of Neuropsychiatry, Graduate of School of Medical Sciences, Maidashi 3-1-1, Higashi-ku, Fukuoka-City, Japan
Dept. of Clinical Radiology, Graduate of School of Medical Sciences, Maidashi 3-1-1, Higashi-ku, Fukuoka-City, Japan
Correspondence: Dr. Monji; e-mail:amonji@hf.rim.or.jp

References

1. Mendez MF, McMurtray A, Chen AK, et al: Functional neuroimaging and presenting psychiatric features in frontotemporal dementia. J Neurol Neurosurg Psychiatry 2006; 77:4–7
2. Woolley JD, Khan BK, Murthy NK, et al: The diagnostic challenge of psychiatric symptoms in neurodegenerative disease: rates of and risk factors for prior psychiatric diagnosis in patients with early neurodegenerative disease. J Clin Psychiatry 2011; 72:126–133
3. Woolley JD, Wilson MR, Hung E, et al: Frontotemporal dementia and mania. Am J Psychiatry 2007; 164:1811–1816
4. Ng B, Camacho A, Lara DR, et al: A case series on the hypothesized connection between dementia and bipolar spectrum disorders: bipolar type VI? J Affect Disord 2008; 107:307–315
5. Mendez MF, Shapira JS, McMurtray A, et al: Accuracy of the clinical evaluation for frontotemporal dementia. Arch Neurol 2007; 64:830–835

nature genetics

A genome-wide association study identifies susceptibility loci for ossification of the posterior longitudinal ligament of the spine

Masahiro Nakajima[1,30], Atsushi Takahashi[2,30], Takashi Tsuji[3,29], Tatsuki Karasugi[1,4], Hisatoshi Baba[5], Kenzo Uchida[5], Shigenori Kawabata[6], Atsushi Okawa[6], Shigeo Shindo[7], Kazuhiro Takeuchi[8], Yuki Taniguchi[9], Shingo Maeda[10], Masafumi Kashii[11], Atsushi Seichi[12], Hideaki Nakajima[5], Yoshiharu Kawaguchi[13], Shunsuke Fujibayashi[14], Masahiko Takahata[15], Toshihiro Tanaka[16], Kei Watanabe[17], Kazunobu Kida[18], Tsukasa Kanchiku[19], Zenya Ito[20], Kanji Mori[21], Takashi Kaito[22], Sho Kobayashi[23], Kei Yamada[24], Masahito Takahashi[25], Kazuhiro Chiba[3,29], Morio Matsumoto[3], Ken-Ichi Furukawa[26], Michiaki Kubo[27], Yoshiaki Toyama[3], Genetic Study Group of Investigation Committee on Ossification of the Spinal Ligaments[28] & Shiro Ikegawa[1]

Ossification of the posterior longitudinal ligament of the spine (OPLL) is a common spinal disorder among the elderly that causes myelopathy and radiculopathy. To identify genetic factors for OPLL, we performed a genome-wide association study (GWAS) in ~8,000 individuals followed by a replication study using an additional ~7,000 individuals. We identified six susceptibility loci for OPLL: 20p12.3 (rs2423294: $P = 1.10 \times 10^{-13}$), 8q23.1 (rs374810: $P = 1.88 \times 10^{-13}$), 12p11.22 (rs1979679: $P = 4.34 \times 10^{-12}$), 12p12.2 (rs11045000: $P = 2.95 \times 10^{-11}$), 8q23.3 (rs13279799: $P = 1.28 \times 10^{-10}$) and 6p21.1 (rs927485: $P = 9.40 \times 10^{-9}$). Analyses of gene expression in and around the loci suggested that several genes are involved in OPLL etiology through membranous and/or endochondral ossification processes. Our results bring new insight to the etiology of OPLL.

OPLL (MIM 602475) is a common disease caused by abnormal ossification of the posterior longitudinal ligament in the spinal canal, affecting 0.8–3.0% of Asians and 0.1–1.7% of European Caucasians[1]. The ossified ligament compresses the spinal cord and nerve root, causing serious neurological dysfunction[2]. Several lines of evidence suggest that genetic factors contribute to its etiology and pathogenesis[3–5]; affected sibling-pair linkage studies and candidate gene association studies have identified a number of genes or loci that are linked to OPLL susceptibility[6–8]. However, replication studies have failed to verify these results, even in the same ancestry groups as the original studies[9]. A GWAS using high-density SNP data has not yet been reported for OPLL.

To identify OPLL susceptibility genes, we conducted a GWAS in a Japanese population consisting of 1,130 individuals with OPLL and 7,135 controls (Online Methods). After quality control filtering of SNP genotyping data (Online Methods), 616,496 autosomal SNPs were examined for association with the Cochran-Armitage trend test. Analysis of population stratification with principal-component analysis (PCA) showed that all individuals in our study were Japanese

[1]Laboratory for Bone and Joint Diseases, Center for Integrative Medical Sciences, RIKEN, Tokyo, Japan. [2]Laboratory for Statistical Analysis, Center for Integrative Medical Sciences, RIKEN, Yokohama, Japan. [3]Department of Orthopaedic Surgery, School of Medicine, Keio University, Tokyo, Japan. [4]Department of Orthopaedic and Neuro-Musculoskeletal Surgery, Faculty of Medical and Pharmaceutical Sciences, Kumamoto University, Kumamoto, Japan. [5]Department of Orthopaedics and Rehabilitation Medicine, Faculty of Medical Sciences, University of Fukui, Fukui, Japan. [6]Department of Orthopaedic Surgery, Tokyo Medical and Dental University, Tokyo, Japan. [7]Department of Orthopedics, Kudanzaka Hospital, Tokyo, Japan. [8]Department of Orthopaedic Surgery, National Okayama Medical Center, Okayama, Japan. [9]Department of Orthopaedic Surgery, Faculty of Medicine, The University of Tokyo, Tokyo, Japan. [10]Department of Medical Joint Materials, Graduate School of Medical and Dental Sciences, Kagoshima University, Kagoshima, Japan. [11]Department of Orthopaedic Surgery, Osaka University Graduate School of Medicine, Osaka, Japan. [12]Department of Orthopedics, Jichi Medical University, Shimotsuke, Japan. [13]Department of Orthopaedic Surgery, Toyama University, Toyama, Japan. [14]Department of Orthopaedic Surgery, Graduate School of Medicine, Kyoto University, Kyoto, Japan. [15]Department of Orthopedic Surgery, Hokkaido University Graduate School of Medicine, Sapporo, Japan. [16]Department of Orthopaedic Surgery, Hirosaki University Graduate School of Medicine, Hirosaki, Japan. [17]Department of Orthopaedic Surgery, Niigata University Medical and Dental General Hospital, Niigata, Japan. [18]Department of Orthopaedic Surgery, Kochi Medical School, Kochi, Japan. [19]Department of Orthopedic Surgery, Yamaguchi University Graduate School of Medicine, Ube, Japan. [20]Department of Orthopedics, Nagoya University Graduate School of Medicine, Nagoya, Japan. [21]Department of Orthopaedic Surgery, Shiga University of Medical Science, Otsu, Japan. [22]Department of Orthopaedic Surgery, National Hospital Organization Osaka Minami Medical Center, Osaka, Japan. [23]Department of Orthopaedic Surgery, Hamamatsu University School of Medicine, Hamamatsu, Japan. [24]Department of Orthopaedic Surgery, Kurume University School of Medicine, Kurume, Japan. [25]Department of Orthopaedic Surgery, Kyorin University School of Medicine, Tokyo, Japan. [26]Department of Pharmacology, Hirosaki University Graduate School of Medicine, Hirosaki, Japan. [27]Laboratory for Genotyping Development, Center for Integrative Medical Sciences, RIKEN, Yokohama, Japan. [28]A full list of members and affiliations appears in the **Supplementary Note**. [29]Present address: Department of Orthopaedic Surgery, Kitasato University Kitasato Institute Hospital, Tokyo, Japan. [30]These authors contributed equally to this work. Correspondence should be addressed to S.I. (sikegawa@ims.u-tokyo.ac.jp).

Received 20 February; accepted 30 June; published online 27 July 2014; doi:10.1038/ng.3045

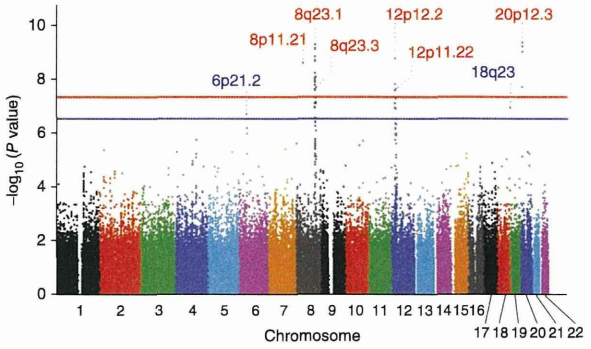

Figure 1 Manhattan plot showing the $-\log_{10} P$ value for each SNP in the GWAS. Values were plotted against their respective positions on the autosomal chromosomes. The red line represents the genome-wide significance threshold ($P = 5 \times 10^{-8}$). The blue line represents the threshold for the selection of SNPs for the replication study ($P = 5 \times 10^{-7}$).

(**Supplementary Fig. 1a**); however, there was a small proportion of samples that were separated from the major Japanese (Hondo) cluster[10] when PCA was performed using only the genotype information for the cases and controls in the study (**Supplementary Fig. 1b**). We used samples from the major Japanese cluster consisting of 1,112 cases and 6,810 controls (**Supplementary Table 1**) and generated a quantile-quantile plot (**Supplementary Fig. 1c**). We found that the genomic inflation factor (λ_{GC}) was 1.01, indicating that there was a low possibility of false positive associations resulting from population stratification. Twenty-six SNPs within six chromosomal regions at 8p11.21, 8q23.1, 8q23.3, 12p12.2, 12p11.22 and 20p12.3 had associations that reached the genome-wide significance threshold of $P < 5 \times 10^{-8}$ (**Fig. 1** and **Supplementary Table 2**). We further found an additional two loci (6p21.2 and 18q23) showing suggestive association with OPLL ($P < 5 \times 10^{-7}$; **Fig. 1** and **Supplementary Table 2**). To investigate additional susceptibility loci, we obtained whole-genome association results for imputed SNPs. We found that 895 SNPs in the 8 identified loci were associated at $P < 5 \times 10^{-7}$, and no other associated loci were uncovered. We also examined 12,228 SNPs on the X chromosome for association with OPLL and found no significant association.

To confirm the associations at the eight loci, we selected the eight SNPs that had the smallest P value at each locus for the replication study. We genotyped an independent set of 548 Japanese individuals with OPLL and 6,469 Japanese controls (**Supplementary Table 1**), finding significant associations for 5 of the 8 SNPs, even after Bonferroni correction with $P < 6.25 \times 10^{-3}$ (0.05/8) (**Table 1** and **Supplementary Table 2**). Combining the results from the GWAS and replication study, six SNPs reached a genome-wide significance threshold of $P < 9.68 \times 10^{-9}$ (0.05/5,163,786) (**Table 1** and **Supplementary Table 3**). The Breslow-Day test for these six SNPs showed an absence of significant heterogeneity ($P > 0.05$) between studies. We carried out age- and sex-adjusted analyses using a logistic regression model and confirmed similar association after adjustment (**Supplementary Table 4**). We next conducted conditional analysis to adjust for the top SNPs at these six loci using the GWAS data. There were no independently associated signals in the six loci (**Supplementary Fig. 2**).

The most highly associated SNP in the meta-analysis, rs2423294 ($P_{combined} = 1.10 \times 10^{-13}$), was located in the 3′ flanking region of *HAO1* at 20p12.3 (**Fig. 2a**). *HAO1* is expressed primarily in the liver and pancreas and encodes hydroxyacid oxidase, which oxidizes 2-hydroxyacid. We identified 80 imputed SNPs in this region that reached a genome-wide significance threshold for association ($P < 5 \times 10^{-8}$); 71 highly associated SNPs ($P < 1 \times 10^{-9}$) were located in the 3′ flanking region of *HAO1* (**Fig. 2a**).

The associated region at 8q23.1 contained three genes—*RSPO2*, *EIF3E* and *EMC2* (**Fig. 2b**). *RSPO2* encodes a member of the R-spondin family of secreted proteins that are involved in β-catenin activation through canonical Wnt/β-catenin signaling[11], which is indispensable for osteoblastogenesis[12]. Reduced expression of R-spondin 2 has been reported in osteoarthritis-derived osteoblasts, and Wnt-dependent mineralization of osteoblasts is promoted by R-spondin 2 (ref. 13). *EIF3E* encodes a component of the eukaryotic translation initiation factor 3 (eIF-3) complex, which is required for several steps in the initiation of protein synthesis. The eIF-3 complex

Table 1 Association of the six genome-wide significant loci

SNP ID	Allele (risk allele)	Chromosome	Genes in or near associated region[a]	Study	RAF Case	RAF Control	P value[b]	OR (95% CI)[c]	P_{het}[d]
rs2423294	T/C (T)	20p12.3	***HAO1***	GWAS	0.207	0.155	4.90×10^{-10}	1.43 (1.27–1.60)	
				Replication	0.203	0.155	4.00×10^{-5}	1.38 (1.19–1.62)	
				Combined[e]	0.205	0.155	1.10×10^{-13}	1.41 (1.29–1.55)	0.757
rs374810	A/G (G)	8q23.1	***RSPO2, EIF3E, EMC2***	GWAS	0.676	0.607	5.79×10^{-10}	1.35 (1.23–1.49)	
				Replication	0.675	0.615	8.88×10^{-5}	1.30 (1.14–1.49)	
				Combined[e]	0.676	0.611	1.88×10^{-13}	1.34 (1.24–1.44)	0.651
rs1979679	T/C (T)	12p11.22	***CCDC91***	GWAS	0.422	0.360	2.42×10^{-8}	1.30 (1.18–1.42)	
				Replication	0.426	0.364	4.75×10^{-5}	1.30 (1.14–1.47)	
				Combined[e]	0.423	0.362	4.34×10^{-12}	1.30 (1.21–1.40)	0.994
rs11045000	A/G (A)	12p12.2	***LOC100506393***	GWAS	0.523	0.454	1.74×10^{-9}	1.32 (1.20–1.44)	
				Replication	0.514	0.466	2.35×10^{-3}	1.21 (1.07–1.37)	
				Combined[e]	0.520	0.460	2.95×10^{-11}	1.28 (1.19–1.38)	0.281
rs13279799	A/G (G)	8q23.3	*LINC00536, EIF3H*	GWAS	0.378	0.317	8.96×10^{-9}	1.31 (1.19–1.44)	
				Replication	0.368	0.322	1.80×10^{-3}	1.23 (1.08–1.39)	
				Combined[e]	0.375	0.319	1.28×10^{-10}	1.28 (1.19–1.38)	0.416
rs927485	T/C (C)	6p21.1	*CDC5L, MIR4642, SUPT3H*	GWAS	0.176	0.134	2.10×10^{-7}	1.37 (1.22–1.55)	
				Replication	0.169	0.140	8.19×10^{-3}	1.25 (1.06–1.48)	
				Combined[e]	0.173	0.137	9.40×10^{-9}	1.33 (1.21–1.46)	0.372

RAF, risk allele frequency; OR, odds ratio; CI, confidence interval.
[a]Genes in the LD block of the associated SNPs are shown in bold. [b]Results from the Cochran-Armitage trend test. [c]Estimated for the risk allele from a 2 × 2 allele frequency table. [d]Results from the Breslow-Day test. [e]Calculated by the Mantel-Haenszel method.

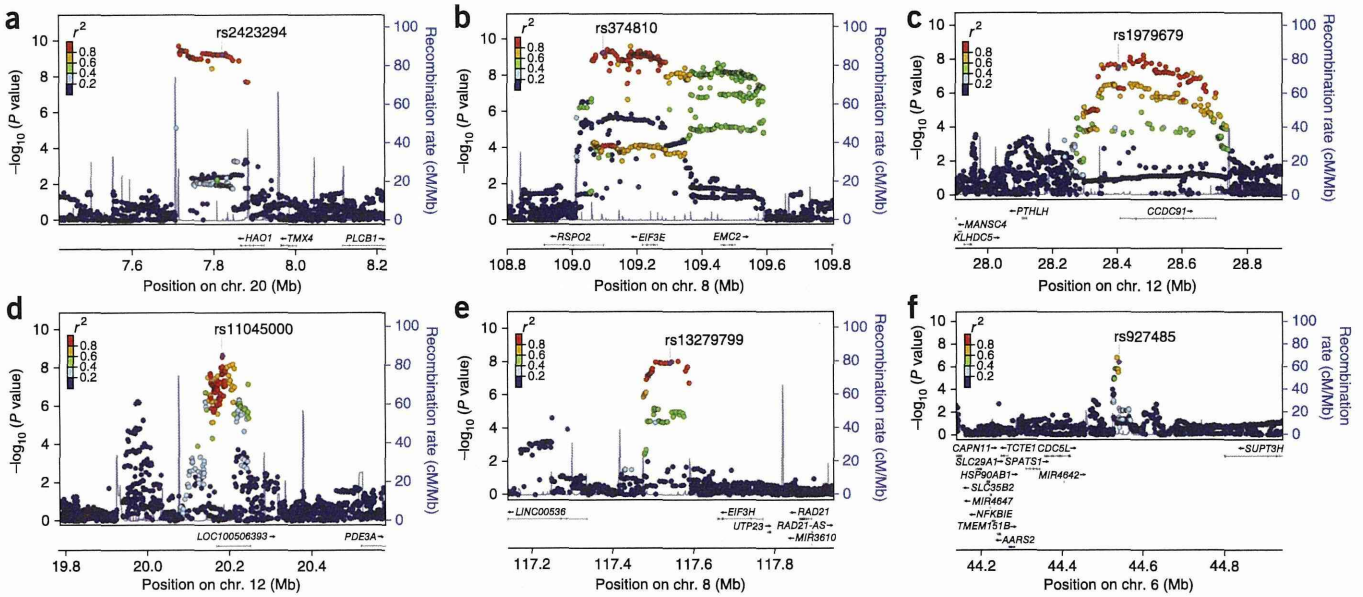

Figure 2 Regional association plots at six susceptibility loci for OPLL. Each plot shows $-\log_{10} P$ values against the chromosomal positions of SNPs in the specific region. The genotyped SNP with the strongest association signal in each locus is represented as a purple diamond; the other SNPs are colored according to the extent of LD with this SNP. Estimated recombination rates from the hg19/1000 Genomes Project March 2012 East Asian reference are shown as light-blue lines. (**a**) 20p12.3. (**b**) 8q23.1. (**c**) 12p11.22. (**d**) 12p12.2. (**e**) 8q23.3. (**f**) 6p21.1.

stimulates mRNA recruitment to the 43S preinitiation complex and scanning of the mRNA for recognition of the translation initiation codon[14]. *EMC2* encodes a component of the endoplasmic reticulum membrane protein complex[15]; however, its cellular function is unclear.

The chromosome 12p11.22 region contained *CCDC91* (**Fig. 2c**), which encodes a protein involved in the trans-Golgi network. Notably, the associated region was located adjacent to the *PTHLH* gene, which encodes a member of the parathyroid hormone (PTH) family. PTH, via its receptor PTH1R, regulates endochondral ossification, which is related to OPLL progression[16]. Associated SNPs at the 12p12.2 locus were in *LOC100506393* (**Fig. 2d**), which is predicted to encode a large intergenic noncoding RNA (lincRNA). *LOC100506393* consists of three exons and has no similarity to known orthologous transcripts. The associated region at 8q23.3 was located in a gene desert between *LINC00536* and *EIF3H* (**Fig. 2e**). *LINC00536* encodes a lincRNA of unknown function. *EIF3H* encodes a component of the eIF-3 complex, as does *EIF3E*. The fact that two of the six loci for OPLL harbor genes encoding proteins in the eIF-3 complex suggests that aberrations in this pathway might be key in OPLL pathogenesis.

The associated region at 6p21.1 was located in the gene desert between *CDC5L*, *MIR4642* and *SUPT3H* (**Fig. 2f**). The cell division cycle 5–like protein encoded by the *CDC5L* gene is a positive regulator of G2/M progression in the cell cycle[17]. CDC5L was also found to be a core component of a putative E3 ubiquitin ligase complex. This complex has been shown to have a role in pre-mRNA splicing from yeast to humans[18]. *MIR4642*, located in intron 14 of the *CDC5L* gene, encodes a microRNA whose target genes and functions are unknown. *SUPT3H* encodes a human homolog of Spt3, which is a *Saccharomyces cerevisiae* transcription factor required for the transcription of a number of RNA polymerase II–transcribed genes[19]. An association of bone mineral density in the lumbar spine with a SNP (rs11755164) 155 kb downstream of the *SUPT3H* gene has been reported[20], but this SNP was not in linkage disequilibrium (LD) with rs927485 ($D' = 0.013$, $r^2 = 0$).

Fifteen genes or loci have previously been reported to be associated with OPLL. We investigated the GWAS data for these reported genes but found no significant association (**Supplementary Table 5**). A genome-wide linkage study reported five loci that showed suggestive linkage after stratification by OPLL severity, age at diagnosis and associated diabetes mellitus[21]. One of the six SNPs that showed genome-wide significant association with OPLL, rs2423294 ($P_{combined} = 1.10 \times 10^{-13}$), was located in the linkage region at 20p12.3 (**Supplementary Fig. 3**). We stratified the cases from our GWAS according to the previous linkage study[21] and investigated the associations of the SNPs in the linkage regions. In all strata, the OR estimates for association increased after stratification (**Supplementary Table 6**). A stratum of subjects without diabetes mellitus showed genome-wide significant association at rs10486860 in the 7q22 linkage region ($P = 4.31 \times 10^{-8}$), suggesting that OPLL is genetically heterogeneous and that the locus is associated with a subtype of OPLL. Association of diabetes mellitus in individuals with OPLL and the contribution of abnormal insulin metabolism to OPLL have been reported[22].

To understand the functional roles of the loci and genes associated with OPLL, we first examined expression of the candidate genes within the LD blocks for the associated SNPs (**Fig. 2**). We assessed the mRNA expression of these six genes in human bone cells and fibroblasts by RT-PCR. *EIF3E*, *EMC2* and *CCDC91* were abundantly expressed in both cells, whereas *HAO1*, *RSPO2* and *LOC100506393* expression was absent in these cells (**Supplementary Fig. 4**). There was no difference in the expression of the genes in the two cell types. We then examined the expression of these genes in the ATDC5 cell line, a mouse model of endochondral ossification[23]. Expression of *Hoa1*, *Rspo2* and *Ccdc91* was lower during early stages of chondrogenesis, whereas expression of *Sox9*, the master gene for chondrogenesis, was higher; in later stages, the expression of cartilage matrix genes (*Acan* and *Col2a1*) was increased (**Supplementary Fig. 5**).

We next investigated the 63 genes within 1 Mb of the associated SNPs for differential expression in osteoblasts and fibroblasts. We examined the cell type–specific gene expression profile using the

FANTOM5 SSTAR database[24]. The expression of four genes was increased by >2-fold in osteoblasts, whereas the expression of six genes was increased by >2-fold in fibroblasts (**Supplementary Table 7**). We examined the ten genes that showed differential expression in quantitative PCR (qPCR) experiments and confirmed increased gene expression of *RSPH9* and *STK38L* in osteoblasts (**Supplementary Table 7**), suggesting that these genes have a role in membranous ossification. The protein encoded by the *RSPH9* gene is a component of the radial spoke head in motile cilia and flagella[25]. The primary cilia machinery has a critical role in the Hedgehog signaling pathway in skeletal development and has been implicated in a dozen disorders known as skeletal ciliopathies[26]. *STK38L* encodes a serine/threonine protein kinase that controls the protein stability of the cyclin-dependent kinase inhibitor protein p21 through direct phosphorylation and inhibits G1/S progression through the cell cycle[27]. We further investigated expression of the 63 genes in mesenchymal stem cells (MSCs) from the spinal ligament. We compared gene expression between the MSCs obtained from subjects with and without OPLL[28] using a cDNA microarray and confirmed differential expression by qPCR. There was no significant difference in the expression of the genes within 1 Mb of the associated SNPs (data not shown).

To gain additional information regarding the function of the SNPs, we examined all publically available expression quantitative trait locus (eQTL) data (Genevar) obtained from the analysis of a lymphoblastoid cell line[29]. There was no evidence of a significant association between genotype and gene expression ($P > 0.05$ after adjustment for multiple testing). We applied literature-based pathway analysis, using GRAIL[30] to investigate the connections between genes in the OPLL-associated loci. We used 6 regions that had a significant genome-wide association as query regions, resulting in the analysis of 12 unique genes. We found a subset of two SNPs with a functional connection (GRAIL $P < 0.05$)—*EIF3E* (rs374810; $P = 0.020$) and *EIF3H* (rs13279799; $P = 0.021$)—with members of the translation initiation pathway.

In summary, through a GWAS and replication study in Japanese populations, we identified six new susceptibility loci for OPLL. One of these overlapped with a previously reported linkage region. Analyses of gene expression in and around the OPLL-associated loci suggested that *RSPH9* and *STK38L* might be involved in OPLL etiology through the membranous ossification process and that *HAO1*, *RSPO2* and *CCDC91* might be involved through the endochondral ossification process. Additional genetic and functional studies for the loci and genes identified by our study should aid in clarification of the etiology and pathogenesis of OPLL.

URLs. 1000 Genomes Project, http://www.1000genomes.org/; Genevar, http://www.sanger.ac.uk/resources/software/genevar/; GRAIL, http://www.broadinstitute.org/mpg/grail/; FANTOM5 SSTAR, http://fantom.gsc.riken.jp/5/sstar/Main_Page; EIGENSTRAT, http://genetics.med.harvard.edu/reich/Reich_Lab/Software.html; Minimac, http://genome.sph.umich.edu/wiki/Minimac; LocusZoom, http://csg.sph.umich.edu/locuszoom/; PLINK, http://pngu.mgh.harvard.edu/~purcell/plink/.

METHODS

Methods and any associated references are available in the online version of the paper.

Note: Any Supplementary Information and Source Data files are available in the online version of the paper.

ACKNOWLEDGMENTS

We thank the individuals with OPLL and their families who participated in this study and the Japan OPLL Network (Zen-Sekichu-Ren), including Ishikawa prefecture OPLL Tomo-no-kai. We also thank Y. Takahashi and T. Oguma for technical assistance. The work reported in this article was supported by grants from the Ministry of Health, Labour and Welfare of Japan: Committee for Study of Ossification of Spinal Ligament (H23-Nanchi-Ippan-032) and Committee for Research and Development of Therapies for Ossification of Posterior Longitudinal Ligament (H26-Itaku(Nan)-Ippan-053).

AUTHOR CONTRIBUTIONS

S.I. designed the project and provided overall project management. M.N. and S.I. drafted the manuscript. M.N. and M. Kubo performed the genotyping for the GWAS. A.T. analyzed the GWAS data. T. Tsuji, T. Karasugi, H.B., K.U., S. Kawabata, A.O., S.S., K.T., Y. Taniguchi, S.M., M. Kashii, A.S., H.N., Y.K., S.F., M. Takahata, T. Tanaka, K.W., K.K., T. Kanchiku, Z.I., K.M., T. Kaito, S. Kobayashi, K.Y., M. Takahashi, K.C., M.M., K.-I.F. and Y. Toyama managed the DNA samples and clinical data.

COMPETING FINANCIAL INTERESTS

The authors declare no competing financial interests.

1. Matsunaga, S. & Sakou, T. in *OPLL: Ossification of the Posterior Longitudinal Ligament* 2nd edn. (eds. Yonenobu, K., Nakamura, K. & Toyama, Y.) 11–17 (Springer, Tokyo, 2006).
2. Matsunaga, S. *et al.* Pathogenesis of myelopathy in patients with ossification of the posterior longitudinal ligament. *J. Neurosurg.* **96**, 168–172 (2002).
3. Sakou, T., Matsunaga, S. & Koga, H. Recent progress in the study of pathogenesis of ossification of the posterior longitudinal ligament. *J. Orthop. Sci.* **5**, 310–315 (2000).
4. Taketomi, E., Sakou, T., Matsunaga, S. & Yamaguchi, M. Family study of a twin with ossification of the posterior longitudinal ligament in the cervical spine. *Spine* **17**, S55–S56 (1992).
5. Okawa, A. *et al.* Mutation in *Npps* in a mouse model of ossification of the posterior longitudinal ligament of the spine. *Nat. Genet.* **19**, 271–273 (1998).
6. Koga, H. *et al.* Restriction fragment length polymorphism of genes of the α2(XI) collagen, bone morphogenetic protein-2, alkaline phosphatase, and tumor necrosis factor-α among patients with ossification of posterior longitudinal ligament and controls from the Japanese population. *Spine* **21**, 469–473 (1996).
7. Nakamura, I. *et al.* Association of the human *NPPS* gene with ossification of the posterior longitudinal ligament of the spine (OPLL). *Hum. Genet.* **104**, 492–497 (1999).
8. Tanaka, T. *et al.* Genomewide linkage and linkage disequilibrium analyses identify *COL6A1*, on chromosome 21, as the locus for ossification of the posterior longitudinal ligament of the spine. *Am. J. Hum. Genet.* **73**, 812–822 (2003).
9. Horikoshi, T. *et al.* A large-scale genetic association study of ossification of the posterior longitudinal ligament of the spine. *Hum. Genet.* **119**, 611–616 (2006).
10. Yamaguchi-Kabata, Y. *et al.* Japanese population structure, based on SNP genotypes from 7003 individuals compared to other ethnic groups: effects on population-based association studies. *Am. J. Hum. Genet.* **83**, 445–456 (2008).
11. Kim, K.A. *et al.* R-spondin proteins: a novel link to β-catenin activation. *Cell Cycle* **5**, 23–26 (2006).
12. Monroe, D.G., McGee-Lawrence, M.E., Oursler, M.J. & Westendorf, J.J. Update on Wnt signaling in bone cell biology and bone disease. *Gene* **492**, 1–18 (2012).
13. Abed, É. *et al.* R-spondins are newly recognized players in osteoarthritis that regulate Wnt signaling in osteoblasts. *Arthritis Rheum.* **63**, 3865–3875 (2011).
14. Chaudhuri, J., Chowdhury, D. & Maitra, U. Distinct functions of eukaryotic translation initiation factors eIF1A and eIF3 in the formation of the 40 S ribosomal preinitiation complex. *J. Biol. Chem.* **274**, 17975–17980 (1999).
15. Christianson, J.C. *et al.* Defining human ERAD networks through an integrative mapping strategy. *Nat. Cell Biol.* **14**, 93–105 (2012).
16. Sato, R. *et al.* Ossification of the posterior longitudinal ligament of the cervical spine: histopathological findings around the calcification and ossification front. *J. Neurosurg. Spine* **7**, 174–183 (2007).
17. Zhang, N., Kaur, R., Akhter, S. & Legerski, R.J. Cdc5L interacts with ATR and is required for the S-phase cell-cycle checkpoint. *EMBO Rep.* **10**, 1029–1035 (2009).
18. Ajuh, P. *et al.* Functional analysis of the human CDC5L complex and identification of its components by mass spectrometry. *EMBO J.* **19**, 6569–6581 (2000).
19. Yu, J., Madison, J.M., Mundlos, S., Winston, F. & Olsen, B.R. Characterization of a human homologue of the *Saccharomyces cerevisiae* transcription factor Spt3 (SUPT3H). *Genomics* **53**, 90–96 (1998).
20. Estrada, K. *et al.* Genome-wide meta-analysis identifies 56 bone mineral density loci and reveals 14 loci associated with risk of fracture. *Nat. Genet.* **44**, 491–501 (2012).
21. Karasugi, T. *et al.* A genome-wide sib-pair linkage analysis of ossification of the posterior longitudinal ligament of the spine. *J. Bone Miner. Metab.* **31**, 136–143 (2013).

22. Kawaguchi, H. *et al.* in *OPLL: Ossification of the Posterior Longitudinal Ligament* 2nd edn. (eds. Yonenobu, K., Nakamura, K. & Toyama, Y.) 71–75 (Springer, Tokyo, 2006).
23. Shukunami, C. *et al.* Chondrogenic differentiation of clonal mouse embryonic cell line ATDC5 *in vitro*: differentiation-dependent gene expression of parathyroid hormone (PTH)/PTH-related peptide receptor. *J. Cell Biol.* **133**, 457–468 (1996).
24. FANTOM Consortium and RIKEN PMI and CLST (DGT). A promoter-level mammalian expression atlas. *Nature* **507**, 462–470 (2014).
25. Castleman, V.H. *et al.* Mutations in radial spoke head protein genes *RSPH9* and *RSPH4A* cause primary ciliary dyskinesia with central-microtubular-pair abnormalities. *Am. J. Hum. Genet.* **84**, 197–209 (2009).
26. Huber, C. & Cormier-Daire, V. Ciliary disorder of the skeleton. *Am. J. Med. Genet. C. Semin. Med. Genet.* **160C**, 165–174 (2012).
27. Cornils, H., Kohler, R.S., Hergovich, A. & Hemmings, B.A. Human NDR kinases control G_1/S cell cycle transition by directly regulating p21 stability. *Mol. Cell. Biol.* **31**, 1382–1395 (2011).
28. Harada, Y. *et al.* Osteogenic lineage commitment of mesenchymal stem cells from patients with ossification of the posterior longitudinal ligament. *Biochem. Biophys. Res. Commun.* **443**, 1014–1020 (2014).
29. Yang, T.P. *et al.* Genevar: a database and Java application for the analysis and visualization of SNP-gene associations in eQTL studies. *Bioinformatics* **26**, 2474–2476 (2010).
30. Raychaudhuri, S. *et al.* Identifying relationships among genomic disease regions: predicting genes at pathogenic SNP associations and rare deletions. *PLoS Genet.* **5**, e1000534 (2009).

ONLINE METHODS

Subjects. The characteristics of each case-control group are shown in **Supplementary Table 1**. OPLL was diagnosed by experienced spinal surgeons from the participating hospitals on the basis of radiographic examination of the spine. Ectopic bone formation of the posterior longitudinal ligament in the cervical region of the spine was evaluated. A total of 1,660 Japanese individuals who had OPLL of more than two vertebra segments were included in this study. We used genome-wide screening data from subjects with 1 of 10 diseases (1,145 with cerebral aneurysm, 1,034 with chronic obstructive pulmonary disease, 811 with endometrial cancer, 1,020 with esophageal cancer, 935 with glaucoma, 1,442 with atopic dermatitis, 1,667 with epilepsy, 1,732 with Graves' disease, 612 with nephrotic syndrome and 1,016 with urolithiasis) unrelated to OPLL in the BioBank Japan Project[31], 978 volunteers from the Osaka-Midosuji Rotary Club in Japan and 887 healthy subjects from the PharmaSNP Consortium for the controls. All individuals gave written informed consent to participate in the study. This research project was approved by the ethical committees at the RIKEN Yokohama Institute.

Genotyping and quality control for GWAS. Genomic DNA was extracted from peripheral blood leukocytes using a standard method. For the GWAS, we genotyped case samples using the Illumina HumanOmniExpressExome BeadChip and control samples using the Illumina HumanOmniExpress BeadChip and the Illumina HumanExome BeadChip. After standard SNP quality control, which excluded SNPs with a call rate of <0.99, SNPs that deviated from Hardy-Weinberg equilibrium ($P < 1 \times 10^{-6}$ in controls) and non-polymorphic SNPs, a total of 616,496 autosomal SNPs were used for further analysis. For sample quality control, we evaluated cryptic relatedness for each sample with an identity-by-state method and removed samples that showed second-degrees relatedness or closer. To examine population stratification in this study, we performed PCA[32] using four reference populations from HapMap data as the reference, including Europeans (CEU), Africans (YRI), Japanese (JPT) and Han Chinese (CHB), with smartpca[32]. We generated the scatterplot, using the top two associated principal components (eigenvectors) to identify outliers who did not belong to the JPT/CHB cluster. Subsequently, we performed PCA using only the genotype information from the case and control subjects without HapMap data to further evaluate population substructure. After performing PCA, we selected 1,112 cases and 6,810 controls within the major Japanese (Hondo) cluster for subsequent analysis. We used the quantile-quantile plot of observed *P* values to evaluate the potential effect of population stratification.

In the replication study, we genotyped 548 individuals with OPLL using a multiplex PCR–based Invader assay (Third Wave Technologies). We recruited 6,469 controls within the Hondo cluster registered in BioBank Japan without OPLL for the replication study. The genotype concordance rate for the six SNPs in **Table 1** between samples genotyped using the Illumina HumanOmniExpressExome BeadChip and the same samples genotyped with the multiplex PCR–based Invader assay was 0.9997.

Statistical analysis. In the GWAS and the replication study, we assessed the association of each SNP with the 1-degree-of-freedom Cochran-Armitage trend test. We calculated OR values and their CIs from a 2 × 2 allele frequency table. We combined data from the GWAS and replication study using the Mantel-Haenszel method and examined heterogeneity between studies using the Breslow-Day test[33]. Regional association plots were generated using LocusZoom[34]. We carried out conditional logistic regression analysis with PLINK v1.07 (ref. 35), adjusting for the top SNPs for each locus to determine whether independently associated SNPs existed.

X-chromosome association study. We performed testing for association on the X chromosome for male and female genotypes separately. For male genotypes, we used 758 cases and 3,988 controls. After quality control as described above, we applied the χ^2 test to the 2 × 2 contingency table for 12,401 SNPs. For female genotypes, we used 354 cases and 2,822 controls and applied the 1-degree-of-freedom Cochran-Armitage trend test for 12,908 SNPs. We combined the male and female association test results for 12,229 SNPs using the inverse normal method[36].

Imputation. We performed genotype imputation within the GWAS using Minimac[37]. We used individuals from the 1000 Genomes Project (phased JPT, CHB and Han Chinese South (CHS) data; March 2012) as reference populations[38]. Because imputation errors are more serious when allele frequencies are low, SNPs with minor allele frequencies of <1% were excluded. SNPs with a low quality of imputation (Minimac software quality score of $R^2 < 0.9$) were also excluded. After quality control, 5,163,786 imputed SNPs were available for analysis. Association tests were performed for dosage with mach2dat[39].

Pathway analysis. We investigated connections between genes in the OPLL-associated loci with GRAIL[30]. We set the parameters as follows: genome assembly, release 22/hg18; HapMap population, JPT + CHB; functional data source, PubMed text (August 2012); gene size correction, off; gene list, all human genes within the database. The rs numbers of the six SNPs listed in **Table 1** were used as a query.

Gene expression analysis. MSCs from the spinal ligaments of individuals with and without OPLL were obtained as previously described[28]. ATDC5 cells (RIKEN Cell Bank) were cultured as previously described[23]. cDNA from MSCs, ATDC5 cells, dermal fibroblast and bone was synthesized for quantitative RT-PCR using the Sensiscript RT kit (Qiagen). Quantitative RT-PCR was performed with a StepOnePlus Real-Time PCR system (Applied Biosystems) using the QuantiTect SYBR Green PCR kit (Qiagen).

Microarray analysis. We analyzed mRNA expression in MSCs from the spinal ligaments of individuals with and without OPLL[28] using the SurePrint G3 Human Gene Expression 8x60K array (Agilent Technologies). For the transcripts whose levels were changed by >2-fold and had a false discovery rate–corrected Welch's *t*-test *P* value of <0.05, we verified the difference in expression by qPCR ($n = 8$ for individuals with and without OPLL).

31. Nakamura, Y. The BioBank Japan Project. *Clin. Adv. Hematol. Oncol.* **5**, 696–697 (2007).
32. Price, A.L. *et al.* Principal components analysis corrects for stratification in genome-wide association studies. *Nat. Genet.* **38**, 904–909 (2006).
33. Breslow, N.E. & Day, N.E. Statistical methods in cancer research. Volume II—the design and analysis of cohort studies. *IARC Sci. Publ.* (82), 1–406 (1987).
34. Pruim, R.J. *et al.* LocusZoom: regional visualization of genome-wide association scan results. *Bioinformatics* **26**, 2336–2337 (2010).
35. Purcell, S. *et al.* PLINK: a tool set for whole-genome association and population-based linkage analyses. *Am. J. Hum. Genet.* **81**, 559–575 (2007).
36. Tukiainen, T. *et al.* Chromosome X-wide association study identifies loci for fasting insulin and height and evidence for incomplete dosage compensation. *PLoS Genet.* **10**, e1004127 (2014).
37. Howie, B., Fuchsberger, C., Stephens, M., Marchini, J. & Abecasis, G.R. Fast and accurate genotype imputation in genome-wide association studies through pre-phasing. *Nat. Genet.* **44**, 955–959 (2012).
38. 1000 Genomes Project Consortium. A map of human genome variation from population-scale sequencing. *Nature* **467**, 1061–1073 (2010).
39. Li, Y., Willer, C.J., Ding, J., Scheet, P. & Abecasis, G.R. MaCH: using sequence and genotype data to estimate haplotypes and unobserved genotypes. *Genet. Epidemiol.* **34**, 816–834 (2010).